(59)

Phase-locked Loop Digital FM Receiver for Wireless Communications

by

Thunyachate Ekvetchavit

Submitted to the Department of Electrical Engineering and Computer Science
in partial fulfillment of the requirements for the degrees of

Bachelor of Science in Computer Science and Engineering

and

Master of Engineering in Electrical Engineering

at the

MASSACHUSETTS INSTITUTE OF TECHNOLOGY

May 1998
[June 1998]

Author .....
Department of Electrical Engineering and Computer Science
May 22, 1998

Certified by .....
Dr. Zoran Zvonar
Systems Group Leader, Analog Devices
Thesis Supervisor

Certified by .....
Amos Lapidoth
Assistant Professor of Electrical Engineering and Computer Science
Thesis Supervisor

Accepted by .....
Arthur C. Smith
Chairman, Department Committee on Graduate Students

Phase-locked Loop Digital FM Receiver for Wireless Communications

by

Thunyachate Ekvetchavit

Submitted to the Department of Electrical Engineering and Computer Science
on May 22, 1998, in partial fulfillment of the
requirements for the degrees of
Bachelor of Science in Computer Science and Engineering
and
Master of Engineering in Electrical Engineering

Abstract

We investigate a non-coherent detection technique based on phase-locked loop (PLL) for wireless communication applications, with an emphasis on Digital Enhanced Cordless Telephone (DECT) system. Performance of the PLL receiver in additive white Gaussian noise (AWGN) and interference-limited environments is simulated and compared to that of the "traditional" non-coherent receivers: limiter-discriminator detector (LD) and differential detector (DD). PLL receiver design, including the selection of PLL parameters and post-detection filtering, is also studied. The results indicate that a well-designed PLL receiver is a better candidate for DECT system than either LD or DD receiver.

Thesis Supervisor: Dr. Zoran Zvonar
Title: Systems Group Leader, Analog Devices

Thesis Supervisor: Amos Lapidoth
Title: Assistant Professor of Electrical Engineering and Computer Science

Acknowledgments

I am deeply grateful to my mentor, Dr. Zoran Zvonar, for his guidance, understanding, encouragement, and friendship. Not only has he advised, he has also given me a big picture of how life in engineering career is. His influence on my future as an engineer is unforgettable.

I also feel indebted to Prof. Amos Lapidoth for his interest in my work. He has given me much guidance and encouragement. His participation as my thesis reader is greatly appreciated. In addition, I thank Peter Katzin at Analog Devices for the fruitful discussions which have resulted in much improvement of the thesis.

I would also like to thank my friends both in Boston and faraway. I thank Mali Chivakul for her supports and company when nights were long and the man was tired. This thesis cannot be completed without her proofreading. I also thank Wanwipa, Poompat, Chalee, Pitiporn, Sutapa, and other TSMIT people for their comments and supports. Heartfelt thanks to Tanya Kamchamnong and Watanee Sriwatanapongse who have filled my life for the past six years. Last but not least, special thanks to friends who have shared my laughs and pains: Marong Phadoongsidhi, Manoj Lohatepanont, Vijak Sethaput, Steve Paik, Paisit Herabut, and Twarath Sutabutr. Their friendships are much appreciated and cherished.

This acknowledgments cannot be completed without my unsurpassed gratitude to my parents and family. Without them, I cannot be here today. This thesis is dedicated to my mom and dad.

Contents

List of Figures

List of Tables

Chapter 1

INTRODUCTION

1.1 Motivation

Continuous Phase Modulation (CPM) describes a class of digital frequency modulation (FM) techniques, which is widely used in mobile radio communications. One particular CPM scheme of interest is Gaussian Minimum Shift Keying (GMSK) modulation introduced by Murota and Hirade in [23]. GMSK is implemented in many wireless applications, including Global System for Mobile (GSM) and Digital Enhanced Cordless Telephone (DECT) systems [11].

The focus of this thesis is a non-coherent detection technique based on phase-locked loop (PLL) for GMSK modulation. Other non-coherent detection techniques, commonly used in mobile radio systems, are limiter-discriminator detection (LD) and differential detection (DD). The performance of both receivers for CPM has been studied extensively in additive white Gaussian noise (AWGN) environment [25] - [32]. On the other hand, no analytical results on the performance of PLL-based detection have been reported because of non-linear characteristics of PLL. Most implementations of the PLL receiver have, therefore, relied on empirical studies [6].

The goal of this thesis is to investigate the performance of the PLL receiver and to provide the design guidelines for wireless communication systems with an emphasis on the DECT framework. Receiver design includes the selection of PLL parameters and post-detection filtering. The major portion of this study is carried out by computer simulations and is supported by analysis based on the linearized PLL model. Error performance of the PLL receiver is compared with that of the limiter-discriminator and differential detector

receivers. The study includes the performance in AWGN environment and interference-limited environment resulting from cochannel and adjacent channel interference.

The rest of this chapter contains the summary of the characteristics of CPM and introduces GMSK and its closely related modulation scheme, Minimum Shift Keying (MSK). An overview of non-coherent digital FM receivers is also given, together with the comparison between non-coherent and coherent detection techniques. Furthermore, we also include an overview of the DECT standard.

In Chapter 2, the detailed description of non-coherent receivers is presented. For LD and DD detection, we highlight the derivation of theoretical performance presented in [26, 29, 30] and the effects of pre-detection and post-detection filtering. For PLL-based detection, we first provide the background on PLL including a linearized model and specific details of a second-order PLL, and subsequently summarize the major characteristics of PLL detector. For each receiver, the complex baseband model which will be used in simulation is described.

In Chapter 3, we first describe the simulation setup, including timing normalization and implementation of the pre-detection and post-detection filters. Using a noise-free signal, we illustrate the three detection techniques. Major part of the chapter is devoted to simulation results of the PLL receiver in AWGN and interference-limited environments. Performance of the PLL receiver is compared to that of the LD and DD receivers. Furthermore, the selection of PLL and post-detection filter parameters is described.

Finally, in Chapter 4, we discuss future works and provide conclusion.

1.2 Continuous Phase Modulation

Continuous phase modulation (CPM) is a class of modulation schemes in which the transmitted signal, $s(t)$, has a general form

$$s(t) = A\cos(2\pi f_c t + \theta(t) + \theta_o) \tag{1.1}$$

where A is the carrier amplitude, f_c is the carrier frequency, and $\theta(t)$ is the transmitted phase. The constant θ_o represents a carrier-phase shift due to transmission delay and is generally assumed to be uniformly distributed between $[-\pi, \pi]$.

For all CPM signals, the transmitted phase, $\theta(t)$, is continuous. Its derivative $\theta'(t)$, the instantaneous frequency, is described by

$$\theta'(t) = 2\pi h \sum_{i=-\infty}^{n} \alpha_i g(t - iT), \qquad nT \le t < (n+1)T \tag{1.2}$$

where T is a symbol period, and $\{\alpha_i\}$ is an M-ary input sequence. The parameter h is known in digital FM literature as a modulation index, and $g(t)$ is called a frequency pulse. Each symbol in the sequence is chosen from an alphabet set $\{\pm 1, \pm 3, \ldots, \pm(M-1)\}$.

The pulse $g(t)$ is positive in a time interval $[0, LT]$ and 0 otherwise, where L is a positive integer. In addition, it is normalized such that

$$\int_{-\infty}^{\infty} g(\tau)d\tau = \int_{0}^{LT} g(\tau)d\tau = \frac{1}{2}. \tag{1.3}$$

Therefore, we obtain

$$\theta'(t) = 2\pi h \sum_{i=n-L+1}^{n} \alpha_i g(t - iT), \qquad nT \le t < (n+1)T \tag{1.4}$$

which indicates that each symbol α_i effects $\theta'(t)$ for L consecutive symbol periods. CPM schemes with $L = 1$ are known as full response CPM. For other values of L, they are called partial response CPM.

Integrating (1.4) from $-\infty$ to t yields

$$\theta(t) = \pi h \sum_{i=-\infty}^{n-L} \alpha_i + 2\pi h \sum_{i=n-L+1}^{n} \alpha_i q(t - iT), \qquad nT \le t < (n+1)T \tag{1.5}$$

where $q(t)$ is a phase pulse defined by

$$q(t) = \int_{-\infty}^{t} g(\tau)d\tau = \begin{cases} 0, & t < 0 \\ \int_{0}^{t} g(\tau)d\tau, & 0 \le t \le LT \\ \frac{1}{2}, & t > LT. \end{cases} \tag{1.6}$$

From (1.5), the expression for $\theta(t)$ can be viewed as a sum of two parts. The first part represents the phase accumulation of all symbols up to α_{n-L}, and the second is a function of the L most recent symbols. Because $\theta(t)$ depends on the entire history of the input sequence, CPM is a modulation scheme with memory. This is a significant distinction from other digital modulation schemes such as pulse amplitude modulation (PAM), frequency shift keying (FSK), and phase shift keying (PSK), where the phase over different signaling periods is statistically independent [15].

By carefully choosing $g(t)$, h, L and M, we can generate a variety of CPM signals. Two CPM schemes of interest are discussed in the next two sections.

1.2.1 Minimum shift keying (MSK) modulation

Minimum shift keying (MSK) is a binary CPM scheme with the modulation index of $\frac{1}{2}$ and a rectangular pulse $g(t)$ defined by

$$g(t) = \begin{cases} \frac{1}{2T}, & 0 \le t \le T \\ 0, & \text{otherwise.} \end{cases} \tag{1.7}$$

Figure 1-1 displays $g(t)$ and the corresponding $q(t)$. From (1.1) and (1.5), an MSK signal can be expressed as

$$s_{MSK}(t) = A\cos(2\pi f_c t + \frac{\pi}{2}\sum_{i=-\infty}^{n-1}\alpha_i + \pi\alpha_n\frac{(t-nT)}{2T} + \theta_o), \qquad nT \le t < (n+1)T. \tag{1.8}$$

It is also possible to view MSK as a special kind of FSK modulation known as continuous-phase frequency shift keying (CPFSK). CPFSK describes a family of CPM schemes in which $g(t)$ is defined by (1.7), and h is arbitrary. MSK is, therefore, a CPFSK scheme with $h = \frac{1}{2}$.

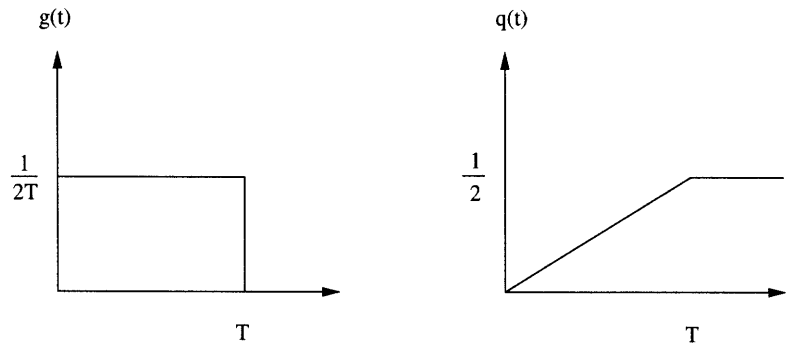

Figure 1-1: Frequency and phase pulses of MSK modulation.

From (1.8), we can write

$$s_{MSK}(t) = A\cos(2\pi(f_c + \alpha_n f_d)\cdot t + (\frac{\pi}{2}\sum_{i=-\infty}^{n-1}\alpha_i - \frac{\pi\alpha_n n}{2}) + \theta_o), \qquad nT \le t < (n+1)T \quad (1.9)$$

where f_d, the peak frequency deviation, is equal to $\frac{h}{2T} = \frac{1}{4T}$. In FSK context, it is the minimum peak frequency deviation which allows a pair of binary FSK signals to be orthogonal. This explains the term "minimum" in MSK [22]. Furthermore, unlike a general FSK modulation, the term $(\frac{\pi}{2}\sum_{i=-\infty}^{n-1}\alpha_i - \frac{\pi\alpha_n n}{2})$ is necessary in $s_{MSK}(t)$ to ensure phase continuity.

By expanding the cosine term in (1.8), we can express $s_{MSK}(t)$ as

$$s_{MSK}(t) = A\cdot\left[a_I(t)\cos(\frac{\pi t}{2T})\cos(2\pi f_c t + \theta_o) - a_Q(t)\sin(\frac{\pi t}{2T})\sin(2\pi f_c t + \theta_o)\right] \quad (1.10)$$

where $a_I(t)$ and $a_Q(t)$ are functions of $\{\alpha_i\}$

$$\begin{aligned} a_I(t) &= \cos(\tfrac{\pi\alpha_n n}{2} - \tfrac{\pi}{2}\sum_{i=-\infty}^{n-1}\alpha_i), && nT \le t < (n+1)T \\ a_Q(t) &= \alpha_n \cdot a_I(t), && nT \le t < (n+1)T. \end{aligned}$$

Equation (1.10) provides another interpretation of MSK as a special type of offset quadrature phase shift keying (OQPSK) modulation. In OQPSK, the bit transition of the quadrature signal, $Q(t)$, is shifted by the bit period, $T_b = T/2$, from the transition of the in-phase

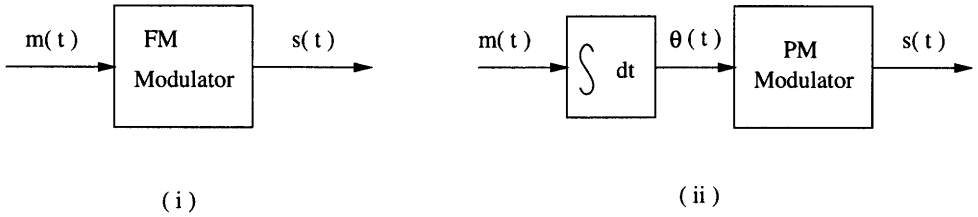

Figure 1-2: MSK modulator implemented according to CPFSK interpretation.

signal, $I(t)$. For $nT_b \leq t < (n+1)T_b$, an OQPSK signal is described by

$$s(t) = \begin{cases} A\,[\alpha_n^I \cos(2\pi f_c t + \theta_o) - \alpha_{n-1}^Q \sin(2\pi f_c t + \theta_o)], & \text{for } n \text{ even} \\ A\,[\alpha_n^I \cos(2\pi f_c t + \theta_o) - \alpha_n^Q \sin(2\pi f_c t + \theta_o)], & \text{for } n \text{ odd} \end{cases} \tag{1.11}$$

where α_n^I and α_n^Q are the n^{th} in-phase (even) and quadrature (odd) input bits respectively [2]. It is apparent that (1.10) is a special case of (1.11) where the rectangular pulse is replaced by the sinusoidal pulses: $\cos(\frac{\pi t}{2T})$ and $\sin(\frac{\pi t}{2T})$.

Since MSK can be considered either as CPFSK or OQPSK modulation, MSK modulation can be implemented by either approach. Relying on the CPFSK description, we can generate MSK signal using a regular FM transmitter where the input signal, $m(t)$, is a rectangular non-return-to-zero (NRZ) waveform with an amplitude $\pm\frac{1}{2T}$ (Figure 1-2 (i)). The modulation index of $\frac{1}{2}$ is achieved by setting $f_d = \frac{1}{4T}$. An MSK signal can also be generated using phase modulation as illustrated in Figure 1-2 (ii). Note that the entire history of the phase is needed in order to derive $\theta(t)$.

Following a discussion on OQPSK, the implementation of an MSK modulator is shown in Figure 1-3. The original bit sequence is divided into two streams of the in-phase (even) and quadrature (odd) bits. The waveforms $a_I(t)$ and $a_Q(t)$ are calculated and multiplied by the sinusoidal terms as described in (1.10). The output is obtained by combining the in-phase and quadrature signals.

MSK modulation has many desirable properties. Like other CPM schemes, it has a constant envelope and, therefore, can avoid the use of linear power amplifier which is difficult and expensive to implement at high frequency [12]. This gives an advantage over linear modulation such as QPSK or QAM which requires linear amplifiers for good performance. Furthermore, MSK also allows non-coherent detection which is not available in QPSK.

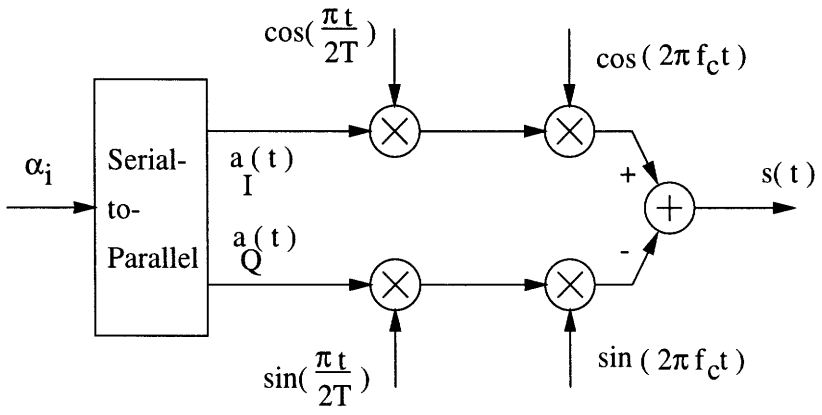

Figure 1-3: MSK modulator implemented according to OQPSK interpretation.

Despite the advantages, MSK is not suitable for mobile radio communications because of its high out-of-band radiation [12, 23]. Nevertheless, we have referred to MSK modulation in detail because we feel that it is necessary for the development of this thesis. In the next section, we present GMSK modulation.

1.2.2 Gaussian minimum shift keying (GMSK) modulation

Introduced by Murota and Hirade in [23], Gaussian minimum shift keying (GMSK) is a modulation scheme closely related to MSK. Historically it was designed for mobile radio communications to achieve smaller sidelobes and better spectral compactness than MSK [23]. Shown in Figure 1-4, better spectral efficiency in GMSK is obtained by filtering an input signal, $m(t)$, with a Gaussian lowpass filter. The impulse response, $h(t)$, of the Gaussian lowpass filter is described by

$$h(t) = \sqrt{\frac{2\pi}{\ln 2}} B_t \cdot \exp\left[-2(2\pi B_t t)^2 / \ln 2\right] \tag{1.12}$$

where B_t is the 3dB bandwidth of the filter [30]. In this study, we are interested in GMSK modulation with $B_t T = 0.5$ because it is employed in DECT systems.

GMSK is also a partial response binary CPM in which $h = \frac{1}{2}$ and

$$g(t) = \frac{1}{2T} \left[h(t) * \mathrm{REC}(t)\right]$$

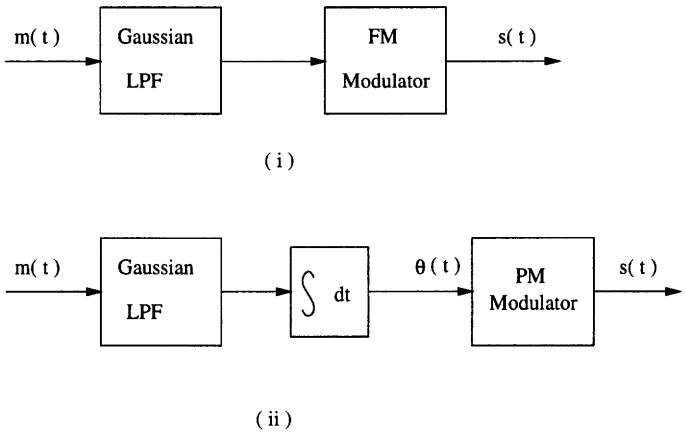

Figure 1-4: GMSK modulator implemented according to CPFSK modulation.

$$= \frac{1}{2T}\left[Q(2\pi B_b \frac{t-T}{\sqrt{\ln 2}}) - Q(2\pi B_b \frac{t}{\sqrt{\ln 2}})\right] \tag{1.13}$$

where $*$ denotes the convolution operation, $\mathrm{REC}(t)$ is a rectangular pulse of duration T, and $Q(x)$ is the error function defined by [15]

$$Q(x) = \int_x^\infty \frac{1}{\sqrt{2\pi}} e^{-\frac{\tau^2}{2}} d\tau.$$

In practice, the pulse $g(t)$ is truncated to an interval $[0, L_T T]$. The truncation is done symmetrically around $t = L_T T/2$, and the new pulse is re-normalized according to (1.3). Also, note that the truncation period L_T depends on the parameter B_t. For $B_t T = 0.5$, we find that setting L_T equal to 4 is appropriate.

Plots of $g(t)$ and $q(t)$ for several GMSK schemes are shown in Figure 1-5. Note that the closed-form expression for $q(t)$ does not exist. Instead, its numerical values are found by integrating $g(t)$ according to (1.6). From the figure, we observe that the shapes of $g(t)$ and $q(t)$ depend on the B_t value. Using smaller B_t results in a more spread-out $g(t)$ and, therefore, higher intersymbol interference (ISI) in the modulation. In other words, the narrower the pre-modulation filter bandwidth is, the higher the level of dependence of GMSK signal on adjacent bits will be. Lastly, we can view MSK as a GMSK modulation with $B_t = \infty$.

In the next section, superior spectral characteristics of GMSK over MSK are displayed. Because of its constant envelope, non-coherent detectability, and high spectral efficiency,

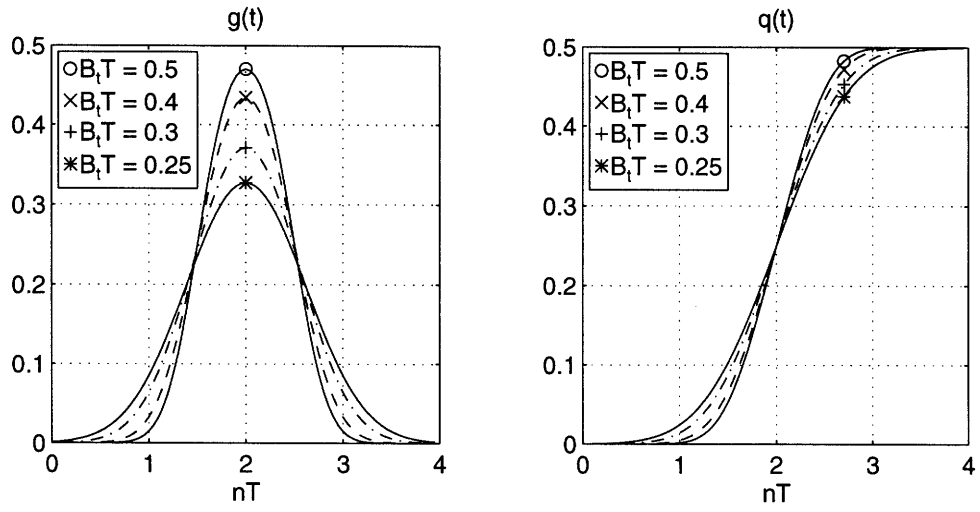

Figure 1-5: Frequency and phase pulses of GMSK signals.

GMSK is widely used in mobile radio communications. Its applications include GSM and DECT systems. Some of the recent Personal Communication System (PCS) standards also employ GMSK modulation [13].

1.2.3 Power spectra of MSK and GMSK signals

In general, the calculation of power spectral density (PSD) of CPM signals is complicated because of the memory in $\theta(t)$ [15]. Closed-form expressions are only available for some CPM schemes. For example, an expression for M-ary CPFSK is given in [2]. For MSK, it can be simplified to [15]

$$S_{lp}(f) = \frac{32E_s}{\pi^2}\left[\frac{\cos(2\pi fT)}{1-16f^2T^2}\right]^2 \tag{1.14}$$

where E_s is the energy per symbol, and $S_{lp}(f)$ denotes the power spectrum of the complex baseband signal of $s_{MSK}(t)$.

For other modulation schemes including GMSK, there are several numerical methods which compute spectral density by time-averaging over an ensemble of transmitted input sequences. Some of these methods are discussed in [2]. In this study, we compute power spectra of GMSK by simulating GMSK signals and applying Welch's averaged periodogram method with Hanning window. This method is discussed in [17]. Figure 1-6 displays spectra of MSK and GMSK signals with $B_tT = 0.3$ and 0.5. The spectrum of the MSK signal is plotted using (1.14). For all signals, the input bits are assumed equiprobable and

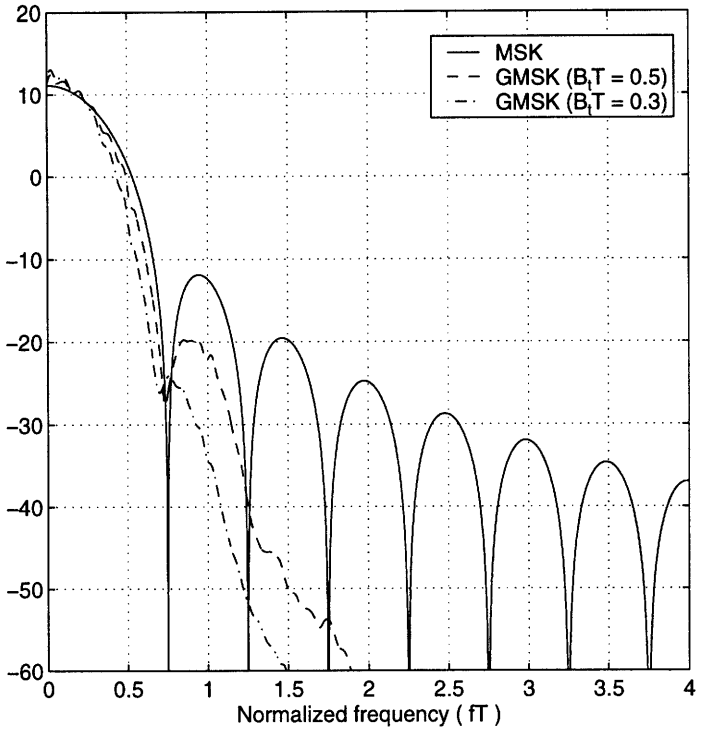

Figure 1-6: Power spectra of MSK and GMSK ($B_tT = 0.3$ and 0.5).

statistically independent.

From Figure 1-6, both GMSK spectra have smaller sidelobes than MSK. In general, because of higher correlation between symbols, a partial response CPM has better spectral characteristics than a full response modulation. In [23], the fractional power ratios of MSK and GMSK signals are given. The 99% total power bandwidth is $1.2R$ for MSK, R for GMSK with $B_tT = 0.5$, and $0.9R$ for GMSK with $B_tT = 0.3$ [23]. The parameter R represents the symbol rate – a reciprocal of T.

1.3 Overview of Non-coherent Digital FM Receivers

1.3.1 System model

In this study, we consider the following structure of non-coherent digital FM receiver shown in Figure 1-7. The receiver consists of a pre-detection filter, a digital FM demodulator, a post-detection filter, a sampler, and a slicer. A transmitted signal, $s(t)$, is corrupted by an additive white Gaussian noise (AWGN) denoted by $n(t)$. In Chapter 4, we add interference

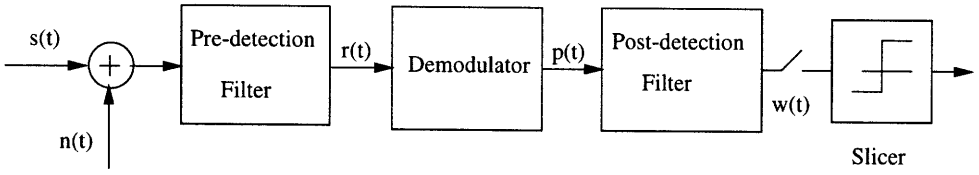

Figure 1-7: Block diagram of a digital FM receiver.

signals typical for wireless systems.

The pre-detection filter is implemented in practice by an Intermediate Frequency (IF) analog filter with a center of passband located at f_c. Its impulse response is denoted by $h_{IF}(t)$, and the corresponding frequency response is $H_{IF}(f)$. Its role is to reduce an out-of-band noise, while passing $s(t)$ with little distortion. A filtered signal, $r(t)$, is demodulated using various detection techniques. Limiter-discriminator detection (LD), differential detection (DD), and PLL-based detection (PLD) are three non-coherent detection methods of interest.

A demodulated signal, denoted by $p(t)$, is then passed through the post-detection filter. The main function of this filter is to attenuate the output noise which increases due to spectral-shaping caused by a demodulator. A filtered signal, $w(t)$, is sampled every T seconds. In this model, we assume that the receiver samples at instants which maximize eye opening of the receiver's noise-free output.

The slicer compares those samples to its threshold and makes a symbol-by-symbol decision. For binary digital FM schemes, the threshold is usually set to zero. However, there are some cases when a non-zero threshold leads to a better performance. One example is the two-bit differential detection discussed in [30].

1.3.2 Effects of pre-detection filtering

In AWGN environment, the output of the pre-detection filter is

$$r(t) = [s(t) + n(t)] * h_{IF}(t). \tag{1.15}$$

For CPM signals, we can show that

$$s(t) * h_{IF}(t) = Aa(t)\cos(2\pi f_c t + \mu(t)) \tag{1.16}$$

where the time-varying amplitude, $a(t)$, and the filtered phase, $\mu(t)$, are

$$a(t) = \sqrt{(h_r(t) * \cos\theta(t))^2 + (h_r(t) * \sin\theta(t))^2} \tag{1.17}$$

$$\mu(t) = \arctan\left(\frac{\sin\theta(t) * h_r(t)}{\cos\theta(t) * h_r(t)}\right). \tag{1.18}$$

In addition, the complex baseband equivalent equation of (1.16) is

$$s_{lp}(t) * h_r(t) = Aa(t)e^{j\mu(t)}. \tag{1.19}$$

The term $h_r(t)$ in (1.17), (1.18), and (1.19) represents the impulse response of the lowpass equivalent of $h_{IF}(t)$. We assume that $h_r(t)$ is real and even. Using properties of Fourier transforms [17], we can derive a relationship between $H_r(f)$, the frequency response of $h_r(t)$, and $H_{IF}(f)$

$$H_{IF}(f) = H_r(f - f_c) + H_r(f + f_c). \tag{1.20}$$

We now discuss the effects of the pre-detection filter on $n(t)$. The noise considered is a zero-mean AWGN with power spectral density $S_n(f) = N_o/2$. An output noise of the pre-detection filter is denoted by $\eta(t)$, where

$$\eta(t) = n(t) * h_{IF}(t). \tag{1.21}$$

Because of the linear time-invariant property of $h_r(t)$, the filtered noise, $\eta(t)$, also has a Gaussian distribution. Its power spectral density and variance are

$$S_\eta(f) = \frac{N_o}{2}|H_{IF}(f)|^2 \tag{1.22}$$

$$\begin{aligned}\sigma_\eta^2 &= \int_{-\infty}^{\infty} S_\eta(f)df \\ &= \frac{N_o}{2} \cdot \int_{-\infty}^{\infty} |H_{IF}(f)|^2 df \\ &= \frac{N_o}{2} \cdot 2\int_{-\infty}^{\infty} |H_r(f)|^2 df \\ &= 2N_o B_{rn}\end{aligned} \tag{1.23}$$

where B_{rn} is the baseband noise-equivalent bandwidth of $h_r(t)$ defined by

$$B_{rn} = \frac{1}{2}\int_{-\infty}^{\infty} |H_r(f)|^2 df. \tag{1.24}$$

Writing $\eta(t)$ in the quadrature form, we obtain

$$\eta(t) = \eta_c(t)\cos 2\pi f_c t - \eta_s(t)\sin 2\pi f_c t \tag{1.25}$$

where $\eta_c(t)$ and $\eta_s(t)$ are the real and imaginary part of the complex baseband noise $\eta_{lp}(t)$. The two waveforms, $\eta_c(t)$ and $\eta_s(t)$, are independent jointly Gaussian random processes [15] with

$$\sigma_{\eta_c}^2 = \sigma_{\eta_s}^2 = \sigma_\eta^2.$$

Combining (1.16) and (1.21), the output of the pre-detection filter is

$$\begin{aligned} r(t) &= Aa(t)\cos(2\pi f_c t + \mu(t)) + \eta(t) \\ &= \mathrm{Re}\{(Aa(t)e^{j\mu(t)} + \eta_{lp}(t))e^{j2\pi f_c t}\}. \end{aligned} \tag{1.26}$$

Thus, its complex baseband signal is given by

$$r_{lp}(t) = Aa(t)e^{j\mu(t)} + \eta_{lp}(t). \tag{1.27}$$

1.3.3 Carrier-to-noise ratio

Carrier-to-noise ratio (CNR) or signal-to-noise ratio (SNR) is a ratio between the signal power and the noise power. Two CNRs of interest are the ratios of signal and noise power measured before and after $h_{IF}(t)$.

By definition of average signal power [9], it is easy to show that

$$\bar{S}_r = \frac{A^2}{2} \tag{1.28}$$

$$\bar{S}_p = \frac{A^2 a^2(t)}{2} \tag{1.29}$$

where $\bar{S}_r$ and $\bar{S}_p$ are the average signal power before and after the filter respectively.

Due to ergodicity of AWGN, average noise power is approximately its variance. Thus

we have already derived the filtered noise power in (1.23). Equivalent expression for the noise power before the filter is

$$\sigma_n^2 = 2\int_{f_c-B_n}^{f_c+B_n} \frac{N_o}{2} df = 2N_oB_n \tag{1.30}$$

where B_n is the lowpass equivalent bandwidth of AWGN $n(t)$.

Therefore, the two CNRs are

$$\rho_r = \frac{A^2/2}{2N_oB_n} \tag{1.31}$$

$$\rho(t) = \frac{a^2(t)A^2/2}{2N_oB_{rn}} \tag{1.32}$$

where we denote the CNR before and after $h_{IF}(t)$ by ρ_r and $\rho(t)$ respectively. Note that $\rho(t)$ is time-varying due to $a(t)$.

Furthermore, by using (1.28) and a relationship between power and energy per symbol, i.e. $\bar{S}_r = E_s/T$, we can show that

$$E_s = A^2T/2. \tag{1.33}$$

Therefore, we can also write the two CNRs in term of E_s

$$\rho_r = \frac{E_s/T}{2N_oB_n} \tag{1.34}$$

$$\rho(t) = \frac{a^2(t)E_s/T}{2N_oB_{rn}}. \tag{1.35}$$

1.3.4 Effects of post-detection filtering

As we mentioned earlier, the main function of the post-detection filter is to attenuate the out-of-band noise while distorting the transmitted signal as small as possible. In classical detection theory, the filter is assumed to be an ideal lowpass filter.

In practice, however, non-ideal filter is implemented. This leads to an increase in inter-symbol interference (ISI), unless the filter satisfies the Nyquist condition [15]. The effects of the post-detection filter depend on pre-detection filter, type of modulation, and demodulation technique. We must, therefore, be careful with the design of post-detection filter along with other components of the receivers. The effects of post-detection filter on each receiver will be discussed when we introduce that particular detection technique.

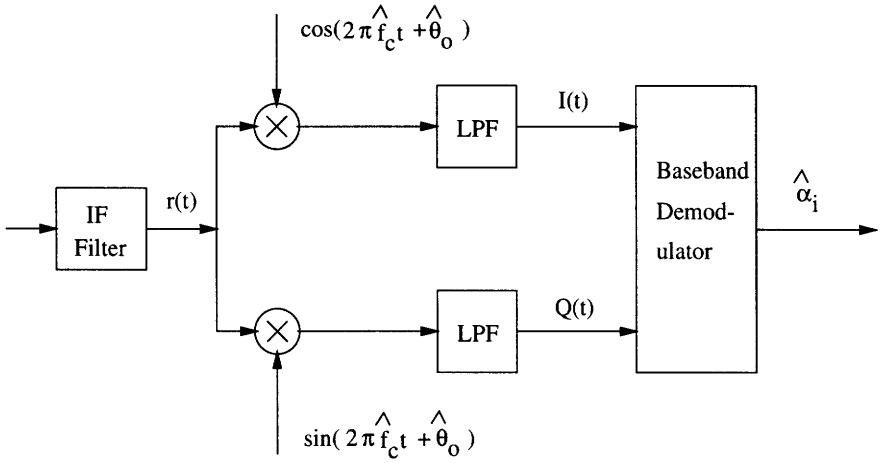

Figure 1-8: Block diagram of a typical coherent receiver.

1.4 Comparison of Coherent and Non-coherent Detection

In coherent detection, the demodulator shown in Figure 1-8 downconverts the filtered signal, $r(t)$, to two baseband signals: the in-phase $I(t)$ and the quadrature $Q(t)$. Further demodulation is then performed on $I(t)$ and $Q(t)$. Since the information about f_c and θ_o is required for the downconversion, a coherent receiver must, therefore, estimates both θ_o and f_c from the received signal. Any mismatch between the estimates and the actual values degrades the receiver performance.

On the other hand, non-coherent detection techniques do not need to recover θ_o. Instead, θ_o is assumed to be uniformly distributed between $[-\pi,\pi]$. Non-coherent detection techniques always perform worse than those employing coherent methods since they do not utilize the phase information. However, in some applications where θ_o rapidly changes, phase recovery is complicated and costly to implement. Therefore, non-coherent detection techniques are more favorable in terms of receiver's complexity and implementation cost in those scenarios.

1.5 Digital Enhanced Cordless Telephone (DECT) Standard

The DECT standard is developed by European Telecommunications Standard Institute (ETSI) with aims to cover a wide range of wireless services from an indoor cordless telephone

to public access systems. DECT is a multi-carrier, time-division multiple access (TDMA) system with channel rate of 1.152 Mbit/sec. Ten frequency carriers are operated in the allocated frequency band from 1,880 MHz to 1,900 MHz with a frequency spacing of 1.728 MHz. In each carrier, TDMA frames of 10 ms are generated where each frame is divided into 24 time slots for uplink and downlink transmission.

The DECT system employs Gaussian Frequency Shift Keying (GFSK) modulation with nominal frequency deviation of 288 KHz. GFSK is GMSK modulation which allows the modulation index to vary in a small range. The normalized bandwidth of the Gaussian filter is $B_tT = 0.5$. In general equalization is not used in DECT receiver. Several implementations of DECT receivers are presented in [33]. The so-called basic DECT receiver is generally based on non-coherent detection using limiter-discriminator.

Chapter 2

NON-COHERENT GMSK RECEIVERS

2.1 Limiter-discriminator Detection

Limiter-discriminator (LD) detection or frequency discriminator detection is widely used in both analog and digital FM systems. Its application includes mobile and satellite communications. Some of the early studies on LD detection of digital FM have been done by Roberts [1], Rice [20], and Mazo and Saltz [21].

The structure of an LD receiver shown in Figure 2-1 consists of two parts: a limiter and a discriminator. The limiter provides constant amplitude of the received signal. The discriminator first extracts the phase from its input and then differentiates the phase waveform. Phase differentiation is essential in the demodulation because the input signal, $m(t)$, is related to the instantaneous frequency of the transmitted signal, $\theta'(t)$, according to (1.2).

In the figure, we denote the extracted phase by $\theta_i(t)$. The output of the discriminator is

$$p(t) = c\frac{d\theta_i(t)}{dt} \tag{2.1}$$

where the constant c is used for amplitude normalization. Assuming that the Laplace transforms of $\theta_i(t)$ and $p(t)$ exist, we can derive the transfer function between the extracted phase and the output of the detector

$$H_{LD}(s) = \frac{P(s)}{\theta_i(s)} = cs \tag{2.2}$$

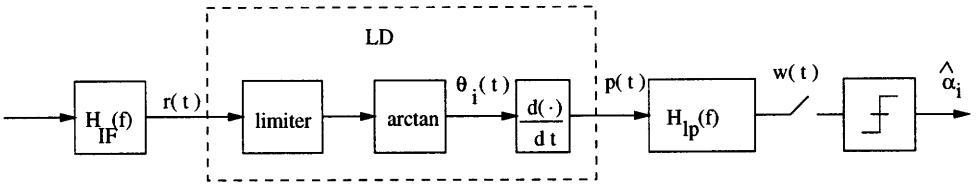

Figure 2-1: Structure of an LD receiver.

where $P(s)$ and $\theta_i(s)$ are the Laplace transforms of $p(t)$ and $\theta_i(t)$ respectively.

From (2.2), the relationship between the power spectrum of $\theta_i(t)$ and $p(t)$ is

$$\frac{S_p(f)}{S_{\theta_i}(f)} = (2\pi c)^2 f^2. \tag{2.3}$$

That is, the power spectrum increases as a quadratic function. This effect, called the quadratic-shaping effect, degrades the performance of the LD detection when the transmitted signal is corrupted by noise and interference because the out-of-band spectrum increases largely. Therefore, a post-detection filter is needed to reduce the unwanted spectrum.

2.1.1 Theoretical performance of LD receiver in AWGN

Theory on the error performance of LD detection in AWGN environment has been presented by Pawula in [26]. This links to an earlier work on click noise theory for analog FM by Rice [20]. By using results from [28], Simon and Wang have later provided a more exact calculation in [29]. The following is the summary of the error performance of the LD detection.

Recall that the complex baseband waveform output of the pre-detection filter is introduced in (1.27)

$$r_{lp}(t) = Aa(t)e^{j\mu(t)} + \eta_{lp}(t).$$

We rewrite it as

$$r_{lp}(t) = Aa(t)\Psi(t)e^{j\mu(t)} \tag{2.4}$$

where a complex waveform $\Psi(t)$ is defined by

$$\Psi(t) = 1 + \frac{\eta_{lp}(t)e^{-j\mu(t)}}{Aa(t)}. \tag{2.5}$$

Simplifying the expression of $r_{lp}(t)$ in (2.4), we obtain

$$r_{lp}(t) = Aa(t)|\Psi(t)|e^{j(\mu(t)+\psi(t))} \tag{2.6}$$

where the magnitude and the phase of $\Psi(t)$ are denoted by $|\Psi(t)|$ and $\psi(t)$ respectively. From (2.6), the filtered IF signal is

$$r(t) = Aa(t)|\Psi(t)| \cos(2\pi f_c t + \mu(t) + \psi(t)). \tag{2.7}$$

The limiter's output has a constant amplitude and is given by

$$A\cos(2\pi f_c t + \mu(t) + \psi(t)). \tag{2.8}$$

Thus, the demodulated signal, which is a derivative of the phase in (2.8), is equal to

$$p(t) = \mu'(t) + \psi'(t). \tag{2.9}$$

Further investigating on $\psi(t)$, we find that

$$\begin{aligned}
\psi(t) &= \arg\left\{1 + \frac{\eta_{lp}(t)e^{-j\mu(t)}}{Aa(t)}\right\} \\
&= \arg\left\{Aa(t) + \eta_{lp}(t)e^{-j\mu(t)}\right\} \\
&= \arg\{Aa(t) + \eta_c(t)\cos\mu(t) + \eta_s(t)\sin\mu(t) \\
&\quad + j[\,\eta_s(t)\cos\mu(t) - \eta_c(t)\sin\mu(t)\,]\,\}
\end{aligned} \tag{2.10}$$

where we use the notation $\arg(x)$ to represent the phase of x.

From (2.10), we can write $\psi(t)$ as the sum of two components

$$\psi(t) = \nu(t) + \varrho(t). \tag{2.11}$$

The first term, $\nu(t)$, is the principal value of $\psi(t)$ defined as

$$\nu(t) = \arctan(\frac{\xi(t)}{A \cdot a(t) + \chi(t)}) \mod 2\pi \tag{2.12}$$

where

$$\xi(t) = \eta_s(t)\cos\mu(t) - \eta_c(t)\sin\mu(t) \tag{2.13}$$

$$\chi(t) = \eta_c(t)\cos\mu(t) + \eta_s(t)\sin\mu(t). \tag{2.14}$$

The second term, $\varrho(t)$, is a step waveform where each jump is approximately equal to $\pm 2\pi$. Note that the range of $\nu(t)$ is $[-\pi, \pi]$, while $\psi(t)$ can take on any values. From (2.11), we can rewrite (2.9) as

$$p(t) = \mu'(t) + \nu'(t) + \varrho'(t). \tag{2.15}$$

Continuous noise The noise $\nu(t)$ in (2.11) is called the continuous noise component of $\psi(t)$. Its probability density function (pdf) is given by [26]

$$p(\nu) = \int_0^\infty dx \frac{x}{\pi} \exp[-(x^2 + \rho(t) - 2x\sqrt{\rho(t)}\cos(\nu))], \qquad \text{for } |\nu| \leq \pi \tag{2.16}$$

where $\rho(t)$ is the CNR after pre-detection filtering defined in Section 1.3.3.

Click noise The term $\varrho'(t)$, which is referred to as 'click noise' in FM literature, is a sequence of impulse-like spikes. A spike with positive (negative) area is called a positive (negative) click. A positive (negative) click occurs when $A \cdot a(t) + \chi(t) < 0$, and $\xi(t)$ changes its sign from positive (negative) to negative (positive) in (2.12). To simplify the calculation, we define a positive and a negative click in terms of Dirac delta function of area 2π and -2π respectively. That is, we define

$$\varrho'(t) = \sum 2\pi\delta(t - t^+) - \sum 2\pi\delta(t - t^-) \tag{2.17}$$

where t^+ and t^- are time instants that positive and negative clicks occur.

Integrate-and-dump filter For the LD detection, the most popular post-detection filter is an integrate-and-dump filter (I&D), which integrates the demodulated output $p(t)$ over

one symbol period and dumps the result to the decision device. The output of the filter is

$$w(t) = \int_{t-T}^{t} p(\tau)d\tau. \tag{2.18}$$

From eq. (14) and (15) of [26], $w(t)$ can be written as

$$\begin{aligned} w(t) &= \mu(t) - \mu(t-T) + [\nu(t) - \nu(t-T)] \bmod 2\pi + 2\pi N(t, t-T) && (2.19) \\ &= \Delta\mu(t) + \Delta\nu(t) + 2\pi N(t, t-T) && (2.20) \end{aligned}$$

where we define $\Delta\mu(t) = \mu(t) - \mu(t-T)$ and $N(t, t-T)$ be a number of clicks in a time interval $[t-T, t]$. The function $[\nu(t) - \nu(t-T)] \bmod 2\pi$, denoted by $\Delta\nu(t)$, is a continuous random variable over $[-\pi, \pi]$. At any time instant, the pdf of $w(t)$ for a particular input sequence is a convolution of the pdf of $\Delta\nu + \Delta\mu$ and the probability mass function (pmf) of $2\pi N(t, t-T)$ as shown in Fig. 3 of [29].

Calculation of error probability Decision rule for the LD detection is the following. First, $w(t)$ is sampled at time instants which maximize eye opening. We denote the sampled $w(t)$ by w. If $w \geq 0$, the receiver decides that a positive bit is sent. Otherwise, it declares the output to be a negative bit. Assuming that each bit is equiprobable, we obtain an average probability of bit error

$$P_e = \frac{1}{2}\,\overline{\Pr}(\{w < 0\}|\text{ a positive bit sent}) + \frac{1}{2}\,\overline{\Pr}(\{w > 0\}|\text{ a negative bit sent}) \tag{2.21}$$

where the average for both terms is taken over all possible data sequences [30].

For GMSK modulation, it has been suggested that taking an average over 5 input bits (two bits before and after the target bit) is sufficient for the modulation with $B_tT \geq 0.2$ [30]. Furthermore,

$$\overline{\Pr}(\{w < 0\}|\text{ a positive bit sent}) = \overline{\Pr}(\{w > 0\}|\text{ a negative bit sent}).$$

Therefore, we simplify (2.21) to

$$\begin{aligned} P_e &= \overline{\Pr}(\{w < 0\}|\text{ a positive bit sent}) \\ &= \tfrac{1}{16}\sum_k \Pr(\{w < 0\}|\ \alpha_k). \end{aligned}$$

The average is taken over 16 possible 5-bit sequences where each has 1 as the target bit [30].

From the pdf of w, denoted by $f_w(w_o)$, it can be shown that, for each α_k,

$$\begin{aligned} \Pr(\{w < 0\}|\ \alpha_k) &= \int_{-\infty}^{0} f_{w|\alpha_k}(w_o|\alpha_k)dw_o \\ &= \Pr(N = 0)\ \Pr(\{-\pi \le \Delta\nu \le -\Delta\mu\}|\alpha_k) \\ &\quad + \sum_{i=1}^{\infty} \Pr(N = i) \end{aligned} \tag{2.22}$$

where $\Pr(N = i)$ is the probability mass function of $N(t, t-T)$ [26].

If the CNR is large and a positive bit is sent, the number of negative clicks will dominate over positive clicks [26]. Thus, positive clicks can be ignored, and the term $N(t, t-T)$ can be regarded as the number of negative clicks in the time interval $[t-T, t]$. The number $N(t-T, t)$ is commonly assumed to be a discrete Poisson random variable with a distribution

$$\Pr(N = k) = \frac{1}{k!}\, e^{-\bar{N}} \bar{N}^k, \qquad k = 0, 1, 2, \ldots \tag{2.23}$$

where $\bar{N}$ is the average number of clicks in the interval $[t-T, t]$. The expression for $\bar{N}$ is given in [26]

$$\bar{N} = \int_{t-T}^{t} \frac{\mu'(t)}{2\pi}\, e^{-\rho(\tau)} d\tau. \tag{2.24}$$

In [30], Simon and Wang apply the result from [28] and suggest that

$$\begin{aligned} \Pr(\{-\pi \le \Delta\nu \le -\Delta\mu\}|\alpha_k) &= \frac{W\sin(\Delta\mu)}{4\pi} \int_{-\pi/2}^{\pi/2} \frac{\exp\left[-\frac{U - V\sin x - W\cos(\Delta\mu)\cos x}{1 - r\cos x}\right]}{U - V\sin x - W\cos(\Delta\mu)\cos x} dx \\ &\quad + \frac{r\sin(\Delta\mu)}{4\pi} \int_{-\pi/2}^{\pi/2} \frac{\exp\left[-\frac{U - V\sin x + W\cos x}{1 + r\cos(\Delta\mu)\cos x}\right]}{1 + r\cos(\Delta\mu)\cos x} dx \end{aligned} \tag{2.25}$$

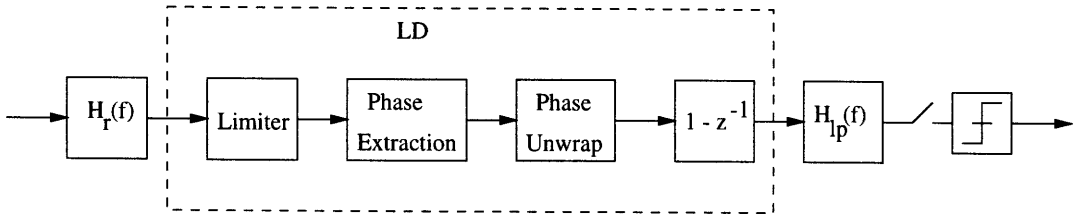

Figure 2-2: Simulation block diagram of an LD receiver.

where U,V, and W are functions of $\rho(t)$

$$\begin{aligned} U &= \tfrac{1}{2}(\rho(t) + \rho(t-T)) \\ V &= \tfrac{1}{2}(\rho(t) - \rho(t-T)) \\ W &= \sqrt{\rho(t)\rho(t-T)} \end{aligned}$$

and r is the normalized noise correlation factor defined by

$$r = \frac{\mathrm{E}[\eta(t)\eta(t-T)]}{\sigma_\eta^2} = \frac{\mathcal{F}^{-1}\{|H_{IF}(f)|^2\}}{\sigma_\eta^2}. \tag{2.26}$$

Substituting (2.24) and (2.25) into (2.22) yields

$$\Pr(\{w < 0\} |\ \alpha_k) = e^{\tilde{N}}\ \Pr(\{-\pi \le \Delta\nu \le -\Delta\mu\}|\alpha_k) + \{1 - e^{\tilde{N}}\}. \tag{2.27}$$

The bit error probability of the LD detection with I&D is then computed by taking the average of (2.27) over 16 possible bit sequences.

2.1.2 Simulation model

Figure 2-2 displays a complex baseband simulation block diagram of an LD receiver. A baseband GMSK signal and an AWGN are first filtered by $h_r[k]$, a discrete-time lowpass equivalent filter of $h_r(t)$. The limiter, in the complex baseband representation, fixes the norm of each received sample to 1. The phase is then extracted from the limited signal and unwrapped by a simple algorithm described in [17]. It has been shown in [14] that this phase unwrapping algorithm improves the performance of the LD detector. Finally, the derivative of the unwrapped phase is taken and passed through the post-detection filter and the decision device.

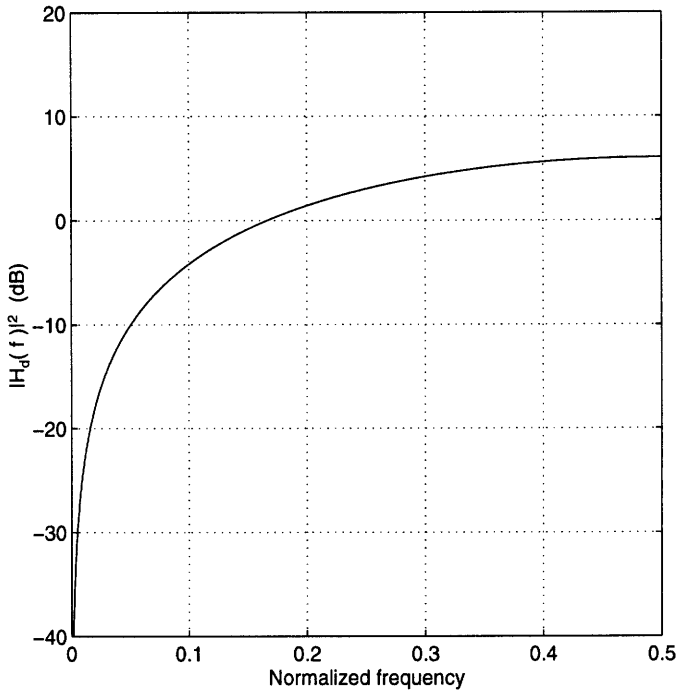

Figure 2-3: Magnitude response of a differentiator.

Phase extraction and phase unwrapping algorithm Phase extraction is done by using a standard arctan function provided in most simulation programs. The output is a principal value of the discrete-time phase, denoted by $\phi[n]$, where $-\pi \leq \phi[n] \leq \pi$.

We then apply the phase unwrapping algorithm to $\phi[n]$. Described in [17], this algorithm corrects phase jumps which are greater than π in absolute value by adding or subtracting 2π to $\phi[n]$ in the opposite direction to the phase jumps. It first computes the difference between the successive phase samples: $\Delta\phi[n] = \phi[n] - \phi[n-1]$. If $|\Delta\phi[n]| > \pi$, $\phi[n]$ is unwrapped by

$$\phi_u[n] = \phi[n] - 2\pi \text{ sign}(\Delta\phi[n]) + \phi_u[n-1] - \phi[n-1]$$

where $\phi_u[n]$ represents the unwrapped phase. Otherwise, the unwrapping algorithm does not add a $\pm 2\pi$ step:

$$\phi_u[n] = \phi[n] + \phi_u[n-1] - \phi[n-1].$$

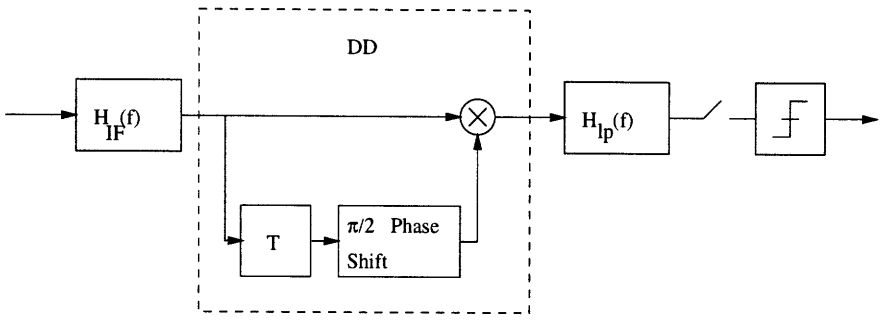

Figure 2-4: Block diagram of a DD receiver.

Implementation of a differentiator In this study, differentiation is done by taking a difference between two successive samples. Its transfer function is

$$H_d(z) = 1 - z^{-1}.$$

It is implemented by a 2-tap FIR filter with the magnitude response displayed in Figure 2-3.

Another possible implementation is by using an FIR filter designed with the Park-McClellan algorithm. Example of this filter has been compared to the simple 2-tap differentiator in [14]; it has been found that both provide the same performance. Since the use of the FIR filter increases computational complexity, we consider only the 2-tap differentiator in our study.

2.2 Differential Detection

Differential detection (DD) was first introduced as a demodulation technique for PSK [31]. It is later used as an alternative to the LD detection in digital FM. Its performance for MSK modulation has been compared to that of the LD detector in [29]. In [30], DD detection of GMSK is investigated [30]. Other studies on DD detection include [25], [31], and [32].

Differential detector first computes a phase difference between the received signal and its delayed version. The delay amount is usually an integer multiple of T, the symbol period. In this study, we emphasize on DD detection with one-bit delay discussed in [29] and [30]. The structure of this receiver is shown in Figure 2-4. Note that the delay branch is phase-shifted by $\pi/2$. Phase comparison is usually done by multiplying the two branches. The output of the DD detector is then filtered by $h_{lp}(t)$ to remove second harmonic terms.

Finally, the slicer makes a symbol-by-symbol decision on the filtered output.

It is interesting to point out that the purpose of the post-detection filter in this receiver is to eliminate the second harmonic term, not the out-of-band noise as in LD detection. We will describe the role of $h_{lp}(t)$ for DD receiver in the next section. Furthermore, in Chapter 3, we confirm this observation by simulating DD receivers with and without $h_{lp}(t)$ and comparing the results.

2.2.1 Theoretical performance of DD receiver in AWGN

From Figure 2-4, the output of the differential detector denoted by $p(t)$ is a product of the filtered signal $r(t)$ and its one-bit delay version with the $\pi/2$ shifted phase. By using the expression for $r(t)$ in (2.7), we obtain

$$\begin{aligned} p(t) &= Aa(t)|\Psi(t)|\cos(2\pi f_c t + \mu(t) + \psi(t)) \times \\ &\quad Aa(t-T)|\Psi(t-T)|\cos(2\pi f_c(t-T) + \mu(t-T) + \psi(t-T) + \pi/2) \\ &= A^2 a(t)a(t-T)|\Psi(t)\Psi(t-T)|\sin(2\pi f_c T + \Delta\mu(t) + \Delta\psi(t)) \end{aligned} \tag{2.28}$$

where $\Delta\mu(t)$ is defined in (2.20) and $\Delta\psi(t) = \psi(t) - \psi(t-T)$. Note that we achieve (2.28) by applying a trigonometric identity

$$\sin(B)\cos(A) = (\sin(A+B) - \sin(A-B))/2 \tag{2.29}$$

and ignoring the second harmonic term. Furthermore, it is assumed that f_c satisfies the following property

$$f_c T = k$$

where k is a positive integer [29]. We can simplify (2.28) to

$$p(t) = A^2 a(t)a(t-T)\ |\Psi(t)|\ |\Psi(t-T)|\sin(\Delta\mu(t) + \Delta\psi(t)). \tag{2.30}$$

Simon and Wang do not specify the type of post-detection filter in [29]. Their assumption is that the filter gets rid of the second harmonic term entirely and leaves the detector's output unchanged. In other words, the output of the receiver denoted by $w(t)$ is exactly $p(t)$ in (2.30).

Similar to the LD receiver, the DD receiver samples $w(t)$ at maximum eye opening instants. The decision rule for this receiver is that a positive bit is sent if $\sin(\Delta\mu + \Delta\psi) > 0$ and a negative bit otherwise. Using the same method of averaging over 16 possible input sequences, we obtain the expression for the error probability for the DD detection

$$\begin{aligned} P_e &= \tfrac{1}{2}\,\overline{\Pr}(\{\sin(\Delta\mu+\Delta\psi)<0\}|\text{ a positive bit sent}) \\ &\quad + \tfrac{1}{2}\,\overline{\Pr}(\{\sin(\Delta\mu+\Delta\psi)>0\}|\text{ a negative bit sent}) \\ &= \overline{\Pr}(\{\sin(\Delta\mu+\Delta\psi)<0\}|\text{ a positive bit sent}) \\ &= \tfrac{1}{16}\sum_k \Pr(\{\sin(\Delta\mu+\Delta\psi)<0\}|\,\alpha_k). \end{aligned}$$

For each α_k, we write $\psi(t)$ in terms of the continuous and click components

$$\begin{aligned} \Pr(\{\sin(\Delta\mu+\Delta\psi)<0\}|\,\alpha_k) &= \Pr(\{\sin(\Delta\mu+\Delta\nu+2\pi N(t,t-T))<0\}|\,\alpha_k) \\ &= \Pr(\{\sin(\Delta\mu+\Delta\nu)<0\}|\,\alpha_k) \\ &= \Pr(\{-\pi\le\Delta\nu\le-\Delta\mu\}|\,\alpha_k) + \\ &\quad \Pr(\{\pi-\Delta\mu\le\Delta\nu\le\pi\}|\,\alpha_k). \end{aligned} \tag{2.31}$$

Comparing the expression of the error probability of the LD detection in (2.27) with that in (2.31), we notice that the continuous component of (2.27) is identical to the first term of (2.31). In addition, there is no click noise effect in DD because of the sine function. However, (2.31) has the second continuous noise component which is not a part of (2.27).

The probability in (2.31) is equal to [29]

$$\begin{aligned} \Pr(\{\sin(\Delta\mu+\Delta\psi)<0\}|\,\alpha_k) &= \frac{W\sin(\Delta\mu)}{4\pi}\int_{-\pi/2}^{\pi/2}\frac{\exp\left[-\frac{U-V\sin x-W\cos(\Delta\mu)\cos x}{1-r\cos x}\right]}{U-V\sin x-W\cos(\Delta\mu)\cos x}dx \\ &\quad + \frac{W\sin(\Delta\mu)}{4\pi}\int_{-\pi/2}^{\pi/2}\frac{\exp\left[-\frac{U-V\sin x+W\cos(\Delta\mu)\cos x}{1+r\cos x}\right]}{U-V\sin x+W\cos(\Delta\mu)\cos x}dx \end{aligned} \tag{2.32}$$

where U,V,W, and r are defined in (2.25). A simpler expression is also given in [29]:

$$\Pr(\{\sin(\Delta\mu+\Delta\psi)<0\}|\,\alpha_k) = \frac{\sqrt{\alpha^2-\beta^2}}{2\pi}\int_0^{\pi}\frac{\exp[-(\alpha-\beta\cos\theta)]}{\alpha-\beta\cos\theta}d\theta \tag{2.33}$$

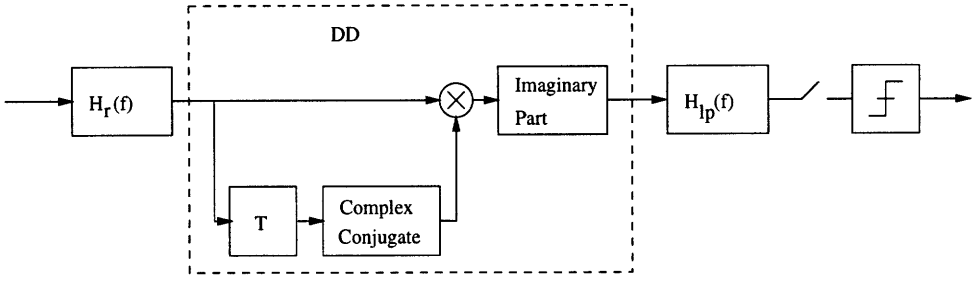

Figure 2-5: Simulation block diagram of a DD receiver.

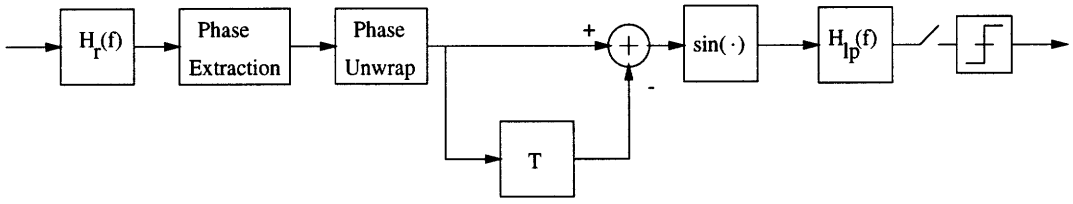

Figure 2-6: Equivalent simulation block diagram of a DD receiver.

where

$$\begin{aligned} \alpha &= (U - rW\cos\Delta\mu)/1 - r^2 \\ \beta &= \sqrt{\alpha^2 - \tfrac{W^2\sin^2\Delta\mu}{1-r^2}}. \end{aligned}$$

2.2.2 Simulation model

Simulation block diagram of a DD receiver is shown in Figure 2-5. Similar to the LD receiver, the complete system is modeled using complex baseband representation. The $\pi/2$ phase shifting in Figure 2-4 is done by taking the complex conjugate of the one-bit delayed version. The imaginary part of the product gives the exact expression as in (2.30). Since the baseband representation ignores all second harmonic terms, there is no need to include the post-detection filter. It is included in Figure 2-5 because we will compare the performance of the DD receiver with and without $h_{lp}(t)$.

2.2.3 Relationship between DD and LD detection

There is an interesting relationship between the LD detection with I&D and the DD detection. The first technique decides that a positive bit is sent if $(\Delta\mu + \Delta\psi) > 0$, while the second checks whether $\sin(\Delta\mu + \Delta\psi) > 0$. Therefore, DD output can be obtained by

applying the sine function to the output of LD with I&D. Figure 2-6 shows the equivalent block diagram of the DD receiver written in the similar fashion to that of the LD receiver.

2.3 PLL-based Detection

Phase-locked loop (PLL) has been widely used in many communication applications, including timing and frequency synchronization, phase extraction, low-power signal reception, and FM demodulation [5]. In analog FM applications, a PLL receiver outperforms a traditional receiver based on LD and, therefore, has been extensively used [6, 10]. Studies of the PLL-based detection of analog and digital FM are given in [4, 5, 6].

2.3.1 Structure of PLL

A PLL consists of three elements: a phase detector, a loop filter, and a voltage-controlled oscillator (VCO). From Figure 2-7, the phase detector produces an output proportional to a difference between the input signal's phase and the VCO signal's phase. This output, called a phase error, is passed through the loop filter whose transfer function is denoted by $F(s)$. The filtered phase error signal is then applied as a VCO's control input. The VCO generates a sinusoidal signal whose phase is proportional to the integral of its control input. To complete the loop, the VCO output is then fed back to the phase detector.

By using the filtered phase error as the input, the VCO changes its frequency in a direction that reduces the phase error. When the error becomes very small and the frequency of the VCO is equal to the average frequency of the input, the loop is "in lock" [6]. Thus, PLL allows the VCO's frequency to track the frequency of the input signal. This frequency tracking ability is one of the most important features of PLL.

We now describe the concept of PLL mathematically. Adapting notations from [6], we denote the input signal's phase by $\theta_i(t)$ and the VCO output's phase by $\hat{\theta}(t)$. The VCO output signal, $v_o(t)$, is a sinusoidal waveform

$$v_o(t) = -\sin(2\pi \hat{f}_c t + \hat{\theta}(t))$$

where $\hat{f}_c$, a carrier frequency of $v_o(t)$, is called the quiescent frequency in [4].

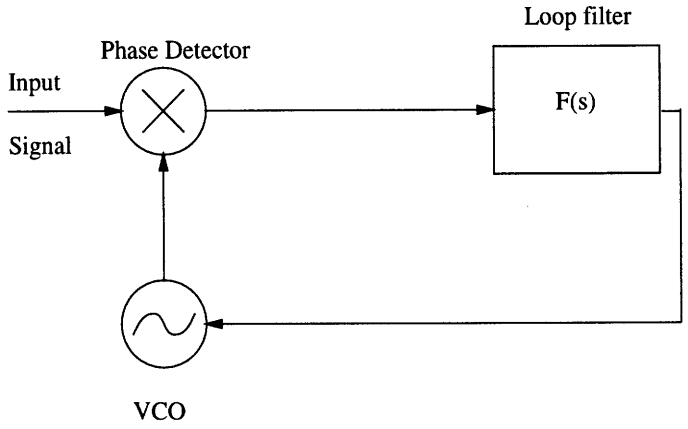

Figure 2-7: Basic structure of a PLL.

The phase detector is generally implemented using a multiplier. Its output, $v_d(t)$, is

$$\begin{aligned} v_d(t) &= C \cdot r(t) \cdot v_o(t) \\ &= CAa(t)\cos(2\pi f_c t + \theta_i(t)) \times -\sin(2\pi \hat{f}_c t + \hat{\theta}(t)) \\ &= \frac{CAa(t)}{2}[\sin(2\pi(f_c - \hat{f}_c)t + \theta_i(t) - \hat{\theta}(t)) - \sin(2\pi(f_c + \hat{f}_c)t + \theta_i(t) + \hat{\theta}(t))] \\ &= K_d Aa(t)[\sin(2\pi(f_c - \hat{f}_c)t + \theta_i(t) - \hat{\theta}(t))] \end{aligned} \tag{2.34}$$

where C is a constant of the multiplier, and $K_d = \frac{C}{2}$ is called a phase detector gain. In (2.34), we are interested in the frequency-difference term only and, therefore, ignore the frequency-sum term. In practice, this is done by using a lowpass filter [6].

In this study, we assume that the phase is always in lock. By setting $f_c = \hat{f}_c$ in (2.34), we obtain

$$v_d(t) = K_d Aa(t)\ \sin(\theta_i(t) - \hat{\theta}(t)). \tag{2.35}$$

The loop filter is a linear time-invariant filter implemented by using lumped circuit elements and operational amplifiers. The transfer function, $F(s)$, is usually a ratio of polynomials

$$F(s) = \frac{V_c(s)}{V_d(s)} \tag{2.36}$$

$$= \frac{a_n s^n + \cdots + a_1 s + a_0}{b_m s^m + \cdots + b_1 s + b_0} \tag{2.37}$$

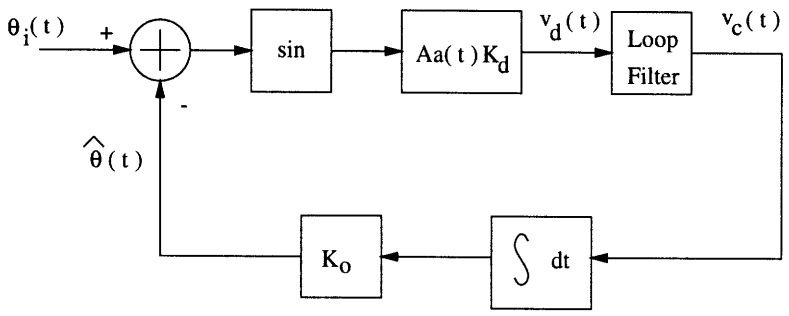

Figure 2-8: Equivalent structure of a PLL.

where $V_c(s)$ and $V_d(s)$ represent the Laplace transforms of $v_c(t)$ and $v_d(t)$ respectively. This transfer function corresponds to the filter's input-output relation in the form of differential equation

$$b_m \frac{d^m v_c(t)}{dt^m} + \cdots + b_1 \frac{dv_c(t)}{dt} + b_o v_c(t) = a_n \frac{d^n v_d(t)}{dt^n} + \cdots + a_1 \frac{dv_d(t)}{dt} + a_o v_d(t). \qquad (2.38)$$

Shown in Figure 2-7, the output of the loop filter, denoted by $v_c(t)$, is fed to the VCO as a control input. Thus, the relationship between $v_c(t)$ and $\hat{\theta}(t)$ is

$$\hat{\theta}(t) = \int_{-\infty}^{t} K_o v_c(\tau) d\tau \qquad (2.39)$$

where K_o is the VCO gain.

From (2.35), (2.38), and (2.39), we can write an equivalent model of PLL shown in Figure 2-8. In this model, the phase detection is done by subtracting $\hat{\theta}(t)$ from $\theta_i(t)$, instead of multiplying $r(t)$ with $v_o(t)$. The VCO is implemented by using an integrator according to (2.39). Note that the demodulator input, $r(t)$, is not directly used in this model. Instead, the phase of $r(t)$ is the input, and the amplitude of $r(t)$ appears in Figure 2-8 as an additional gain factor. In this model, the loop filter remains unchanged.

In summary, we have outlined the basic structure of a PLL and described its main components. The equivalent block diagram is shown in Figure 2-8. We should emphasize again that this model is based on the assumption that the loop is in lock. If not, the term $2\pi(f_c - \hat{f}_c)t$ would not be equal to 0, and we could not use (2.35) to simplify the calculation.

2.3.2 Linearized model

Because of the sine function in (2.35), PLL is a non-linear device. Its analysis in the presence of noise is, therefore, very difficult. In many applications, a linearized model of PLL is implemented instead. This model closely approximates the actual PLL when the phase error, $\theta(t) - \hat{\theta}(t)$, is small.

Considering the case when the amplitude, $A \cdot a(t)$, is equal to a constant A, and the phase error is small, we can modify (2.35) to

$$v_d(t) = K_d A \left(\theta_i(t) - \hat{\theta}(t)\right) \tag{2.40}$$

since $\sin(\theta) \approx \theta$, for small θ.

Further assuming that the Laplace transforms of $\theta_i(t)$, $\hat{\theta}(t)$, $v_c(t)$, and $v_d(t)$ exist, we can write (2.39) and (2.40) in terms of their transforms

$$\hat{\theta}(s) = \frac{K_o V_c(s)}{s} \tag{2.41}$$

$$V_d(s) = K_d A \left(\theta_i(s) - \hat{\theta}(s)\right). \tag{2.42}$$

From (2.36), (2.41), and (2.42), the transfer function between $\hat{\theta}(s)$ and $\theta_i(s)$ is

$$H(s) = \frac{\hat{\theta}(s)}{\theta_i(s)} = \frac{AKF(s)}{s + AKF(s)} \tag{2.43}$$

where K represents the overall gain defined by

$$K = K_o K_d.$$

This function is known in control theory as the closed-loop transfer function. Later, we will use it to describe the PLL-based detection.

2.3.3 Second-order PLL

Most characteristics of PLL such as frequency tracking, phase and frequency acquisition, and loop's stability depend on the loop filter. When $F(s)$ is a constant, the loop is called a first-order PLL because its closed-loop transfer function has 1 pole. A second-order loop then corresponds to a PLL with a 2-poles transfer function. Because of its simple design and

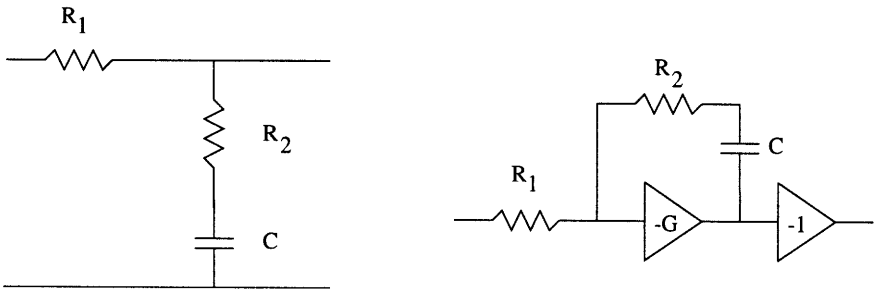

(i) Passive filter

(ii) Active filter

Figure 2-9: Two loop filter implementations for a second-order PLL.

good performance, the second-order PLL is widely used in most applications [6]. Higher-order loops are more complicated and do not necessarily provide improved performance. In this study, we consider only the second-order PLL.

The loop filter for the second-order PLL has a general form of

$$F(s) = \frac{cs + d}{as + b}. \tag{2.44}$$

Figure 2-9 shows two types of the loop filter: a passive and an active. The passive loop filter consists only of lumped circuit elements and has the transfer function

$$F_p(s) = \frac{sR_2C + 1}{s(R_1 + R_2)C + 1}.$$

On the other hand, an active loop filter requires a high-gain amplifier and lumped elements. Its transfer function is

$$F_a(s) = \frac{sCR_2 + 1}{sCR_1}$$

where the gain G in Figure 2-9 is assumed to be high.

It is known that a PLL with an active loop filter has better tracking capability than that with a passive filter [6]. However, a more expensive and complicated circuit is needed. A PLL with a passive filter is easier to implement and performs fairly well in many applications. In this study, we consider a passive-filter PLL where the product of the overall loop gain,

K, and the amplitude of the input signal, A, is much greater than $1/R_2C$. That is,

$$AK \gg \frac{1}{R_2C}.$$

A PLL that satisfies this condition is called a high-gain loop [6].

By substituting $F_p(s)$ into (2.43) and using the high-gain condition, we obtain

$$H(s) = \frac{\frac{AK(sR_2C+1)}{(R_1+R_2)C}}{s^2 + s\frac{AKR_2C}{(R_1+R_2)C} + \frac{AK}{(R_1+R_2)C}}. \tag{2.45}$$

In practice, the second-order PLL is specified in terms of loop parameters instead of circuit elements. Three loop parameters are the overall loop gain K, a damping factor ζ, and a natural frequency w_n. Both ζ and w_n are well-known parameters in second-order systems. In the context of high-gain PLL, they are related to the lumped circuit elements by

$$w_n = \sqrt{\frac{AK}{(R_1 + R_2)C}} \tag{2.46}$$

$$\zeta = \frac{1}{2} R_2C\, w_n. \tag{2.47}$$

Therefore, the closed-loop transfer function of the high-gain second-order PLL is

$$H(s) = \frac{2\zeta w_n s + w_n^2}{s^2 + 2\zeta w_n s + w_n^2}. \tag{2.48}$$

In Figure 2-10, examples of the closed-loop transfer functions are plotted as a function of ζ. The horizontal axis is the frequency, normalized according to $2\pi f/w_n$. From the plots, these transfer functions have lowpass characteristics. The lower the ζ is, the steeper the attenuation becomes. Furthermore, every loop response has a peak above 0 dB near $f = w_n/2\pi$, and a loop with small ζ has a high peak. Following the terminology in second-order linear systems, we refer to a PLL with $\zeta < 1$ as an underdamped loop. In second-order linear systems, the system is underdamped when the transfer function has complex poles. This is equivalent to $\zeta < 1$ in (2.48). More details on second-order linear systems are given in [18].

We should note that the discussion on transfer functions of second-order PLL assumes the linearized model. For an actual PLL, the transfer functions do not exist because of the

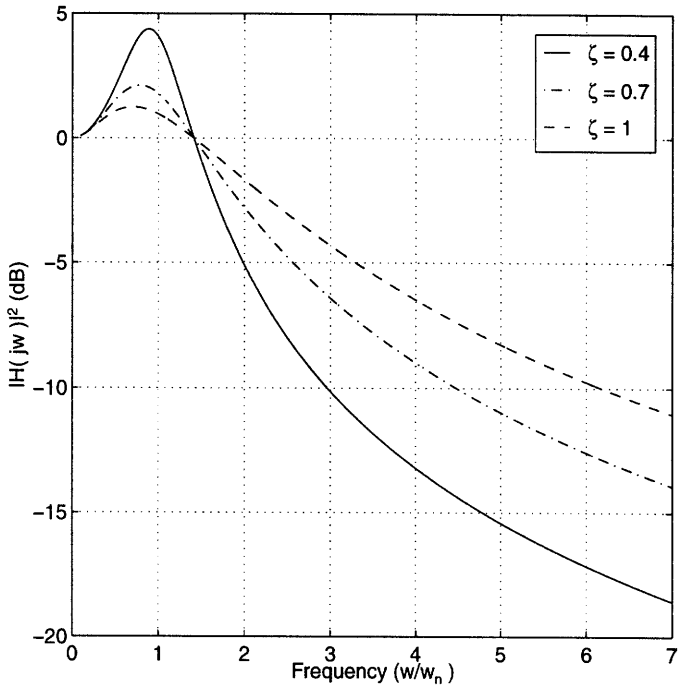

Figure 2-10: Closed-loop transfer function of a high-gain second order PLL.

sine function in (2.35). Nevertheless, we use the linearized model in this study to simplify our analysis. The only exception is in simulation where we implement a non-linear PLL.

2.3.4 PLL demodulator

As mentioned in Section 2.3.1, $\hat{\theta}(t)$ is approximately $\theta_i(t)$ when the loop is locked. Therefore, a derivative of $\hat{\theta}(t)$, $v_c(t)$, should follow the instantaneous frequency of the input signal. Consequently, it can be used as a demodulated output of both analog and digital FM. Detection technique based on phase-locked loop is known as PLL demodulation.

The structure of a PLL demodulator (PLD), shown in Figure 2-11, consists of a limiter and a PLL. The demodulated signal is taken from the output of the loop filter. We include the limiter so that the PLL input has a constant amplitude. As a result, the closed-loop transfer function of the linearized PLL is time-invariant. Without the limiter, $H(s)$ would be time-varying due to the time-varying gain (see Figure 2-8).

From (2.36), (2.41), and (2.42), we can derive the transfer function of the PLL demodulator:

$$H_{PLD}(s) = \frac{P(s)}{\theta_i(s)} = \frac{sH(s)}{K_o} \tag{2.49}$$

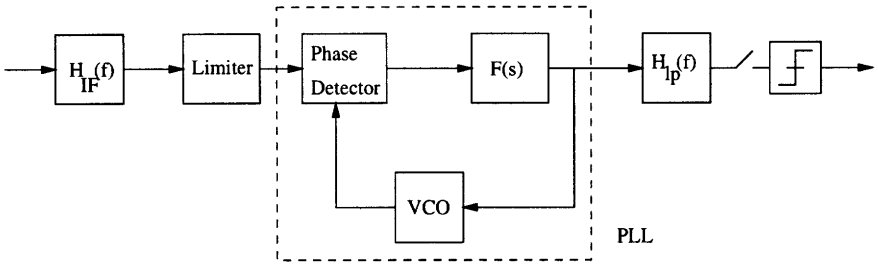

Figure 2-11: Structure of a PLL receiver.

where $P(s)$ is the Laplace transform of $p(t)$, K_o is the VCO gain factor, and $H(s)$ is the closed-loop transfer function in (2.48).

Equation (2.49) provides another interpretation of the PLD detection. Comparing between $H_{LD}(s)$ in (2.2) and $H_{PLD}(s)$, we can view the PLD detection as the LD detection followed by an additional filter whose transfer function is proportional to $H(s)$. Because of its lowpass characteristic, $H(s)$ reduces the quadratic-shaping effect of the differentiator discussed in Section 2.1. Therefore, the high frequency out-of-band noise does not increase in the PLD detection as much as in the LD detection.

Figure 2-12 displays the transfer functions of the PLL demodulators compared to $H_{LD}(s)$ in (2.2). The constant c in $H_{LD}(s)$ and K_o in $H_{PLD}(s)$ are set such that the amplitudes of both demodulated outputs are equal. The frequency is normalized to the bit rate R. From the figure, the magnitude responses of the PLDs are higher than that of the LD at frequency below R because of the peak above 0 dB of the closed-loop transfer functions in Figure 2-10. At higher frequency, however, the responses of all three PLDs are smaller. At $f = 2.5R$, the difference between the responses of the LD and the PLD with $\zeta = 1$ and $F_{3dB} = R$ is 10 dB. This reduction in high frequency noise-shaping is the key to the performance improvement of the PLD detection over the LD detection.

We have mentioned in the previous section that we usually specify the second-order PLL by K, ζ, and w_n. In this study, instead of w_n, we specify the PLL receiver by the closed-loop 3dB bandwidth, F_{3dB}, defined as a frequency such that

$$|H(j2\pi F_{3dB})|^2 = \frac{1}{2}.$$

We should note that there is no particular reason to choose F_{3dB} parameter over w_n. We

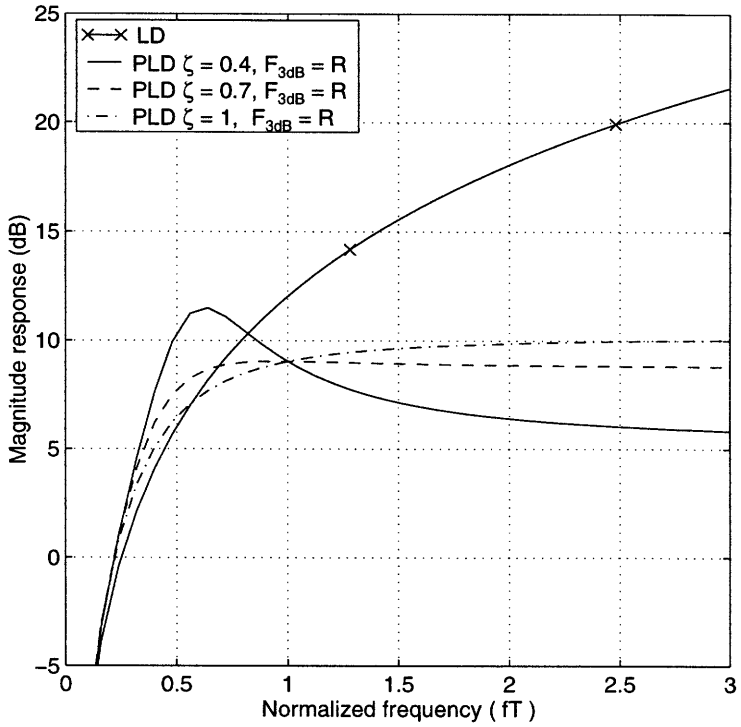

Figure 2-12: Transfer function of a PLD detector compared to a LD detector

use F_{3dB} simply because it reinforces the interpretation of the PLD detection previously discussed.

Lastly, for the high-gain second-order loop, the expression of F_{3dB} in terms of w_n is given by [6]

$$F_{3dB} = \frac{w_n}{2\pi}[2\zeta^2 + 1 + \sqrt{(2\zeta^2+1)^2+1}]^{\frac{1}{2}}. \tag{2.50}$$

2.3.5 Simulation model

The complex baseband model of the high-gain second-order PLL receiver is shown in Figure 2-13. The phase detector is modeled as a complex multiplier. We take the imaginary part of the product to obtain the sine function of the phase error as described in (2.35). The received signal's amplitude is fixed because of the limiter. The loop's discrete-time filter response $F(z)$ is obtained from the passive loop filter, $F_p(s)$, by the bilinear transform

$$F(z) = F_p(s)\big|_{s=2\frac{(1-z^{-1})}{(1+z^{-1})}}.$$

The integration in (2.39) is implemented in discrete time by Forward Euler formula [8],

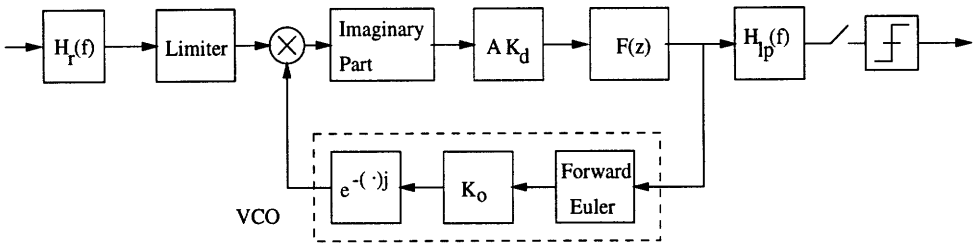

Figure 2-13: Simulation block diagram of a PLL receiver.

where the input-output ($x[n]$-$y[n]$) relation is

$$y[n] = \Delta t x[n-1] + y[n-1]. \tag{2.51}$$

The parameter Δt is the sampling period of the discrete-time system. Finally, the exponential function after the integrator generates a complex baseband VCO output which is fed back to the phase detector.

2.4 Summary

We have described fundamental concepts of the three non-coherent receivers, including their simulation models. For the DD detection and the LD detection with I&D filter, the error performance in AWGN environment has been analyzed in [26, 29, 30]. We summarize the analysis in Section 2.1.1 and Section 2.2.1.

For the PLD detection, we consider only a high-gain second-order PLL. The background on PLL including the linearized model and the second-order loop is presented. By comparing $H_{PLD}(s)$ to $H_{LD}(s)$, we can view the linearized PLD detection as the LD detection combined with an additional lowpass filter. This property leads to the reduction in spectral-shaping and, therefore, better error performance.

Chapter 3

PERFORMANCE OF PLL-BASED GMSK RECEIVER

3.1 Simulation Outline

In Figure 3-1, we illustrate a complex baseband simulation block diagram of GMSK modulation and demodulation. The modulator generates the noise-free signal $s[k]$ from the random input bit sequence. Each bit is equiprobable and independent from one another. Decision timing is determined by plotting the eye diagram of the demodulated noise-free output.

We simulate this communication system in two scenarios. First, we concentrate on the AWGN environment where the transmitted signal is corrupted by an AWGN. Second, we concentrate on the interference-limited environment where cochannel interference and adjacent channel interference are added to the transmitted signal. The output of the pre-detection filter, demodulator, and the post-detection filter are denoted by $r[k]$, $p[k]$, and

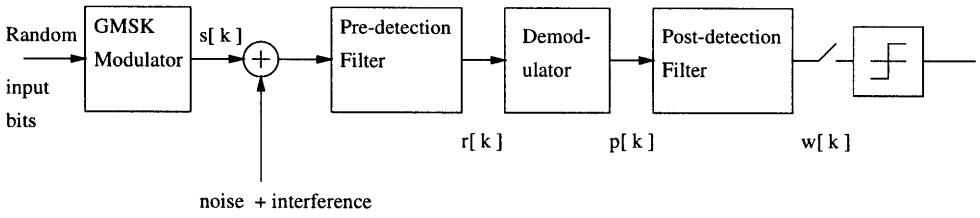

Figure 3-1: Simulation block diagram of GMSK modulation and demodulation.

$w[k]$ respectively.

Before presenting simulation results, we discuss simulation parameters and implementation of the pre-detection and post-detection filters.

3.1.1 Timing normalization

In this study, simulations are done on discrete-time samples of continuous-time signals defined as

$$x[n] = x(n\Delta t)$$

where Δt is the sampling period. For simplicity, the sampling frequency denoted by F_s – a reciprocal of Δt – is normalized to 1. The bit rate and the bit period are denoted by R and T. A parameter $n_s = \frac{T}{\Delta t}$, which represents the number of samples in one bit period, is chosen to be an integer. For all simulations, we select $n_s = 8$ to provide accurate representation of continuous-time systems. In summary, the timing normalization is

$$\begin{aligned} F_s &= \tfrac{1}{\Delta t} = 1 \\ R &= \tfrac{1}{T} = \tfrac{1}{8} \\ n_s &= \tfrac{T}{\Delta t} = 8. \end{aligned}$$

3.1.2 Relationship between CNR and E_b/N_0

For all binary digital transmissions, probability of bit error or bit error rate (BER) is a common performance criteria. In detection theory, the BER in AWGN environment is computed as a function of the ratio between the energy per bit, E_b, and the noise power spectral density, N_o. Performance comparison between different systems is usually done by considering the required E_b/N_o to achieve the certain BER. While the error probability is defined as a function of E_b/N_o, simulation results usually display it as a function of CNR. We now derive the relationship between E_b/N_o and CNR.

From (1.34), the relationship between the CNR before the pre-detection filter, ρ_r, and E_s is

$$\rho_r = \frac{E_s/T}{2N_oB_n}.$$

Since $E_b = E_s$ for GMSK and all binary CPMs, we obtain

$$\rho_r = \frac{E_b/T}{2N_oB_n} = \frac{E_b/N_o}{2TB_n}. \tag{3.1}$$

This connection between E_b/N_o and ρ_r is necessary for deriving the relationship between the simulated BER and E_b/N_o.

3.1.3 Monte Carlo method for calculating BER

The simulation of the BER in this study is based on the Monte Carlo approach where the BER is estimated by the ratio between the number of errors and the total number of bits sent. The simulated BER is a random variable whose mean approaches its true value, when a number of input bits sent is large [8].

The range of BERs of interest is from 10^{-2} to 10^{-4}, with an emphasis at 10^{-3}. For large BERs from 10^{-2} to $2 \cdot 10^{-3}$, the number of input bits are set such that 80 - 400 errors occur. However, only 40 - 60 errors are simulated for lower BERs due to the large number of bits needed. Assuming that errors are independent, we can show that, by the Gaussian approximation, simulating 40 errors produces a 95% confidence interval $[.73\hat{P}_e, 1.36\hat{P}_e]$ where $\hat{P}_e$ is an estimated BER [8]. This means that there is a probability of 0.95 that the true value of BER falls in this interval. With 400 errors, the 95% confidence interval is $[.9\hat{P}_e, 1.1\hat{P}_e]$.

3.1.4 Pre-detection filter

For pre-detection filtering, we choose a family of Gaussian filters described in Section 1.2.2. Similarly, it has been used in [26, 29, 30]. The impulse and frequency response of the lowpass equivalent filter are

$$h_r(t) = \sqrt{\frac{2\pi}{\ln 2}} B_r \exp\left[-2(2\pi B_r t)^2/\ln 2\right] \tag{3.2}$$

$$H_r(f) = \exp\left[-(\frac{\ln 2}{2} f^2)/B_r^2\right] \tag{3.3}$$

where B_r is the 3dB bandwidth of $h_r(t)$. In practice, it is more common to specify a Gaussian pre-detection filter by its IF 3dB bandwidth, denoted by B_{IF}, where $B_{IF} = 2B_r$.

In this study, $h_r(t)$ is implemented as an FIR filter. The discrete-time impulse response is obtained by sampling $h_r(t)$ with the rate F_s and then truncating the number of samples

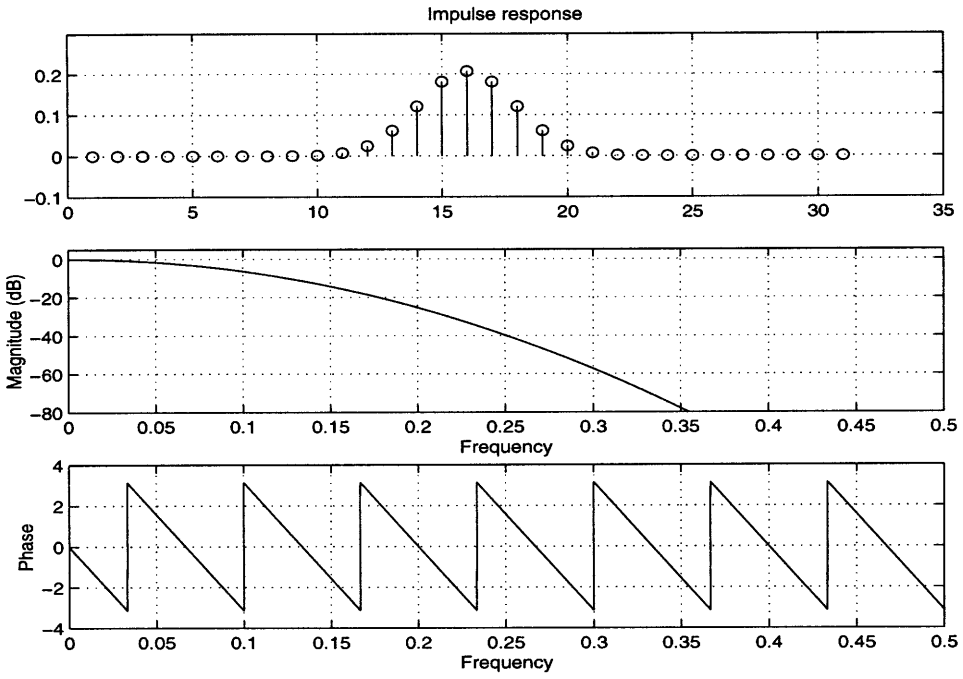

Figure 3-2: Impulse and frequency response of a 31-tap Gaussian pre-detection filter with $B_{IF} = 1.1R$.

to $(L_T \cdot n_s - 1)$. The integer L_T is selected to be large enough such that the truncated filter still has a Gaussian-shape frequency response. We find that $L_T = 4$ is sufficient for $B_{IF} > 0.5R$. A Gaussian filter with $B_{IF} = 1.1R$ and $L_T = 4$ is shown in Figure 3-2. Note that the number of taps for this filter is 31 because n_s is equal to 8.

3.1.5 Post-detection filter

Three different types of lowpass filters are implemented for post-detection filtering: a Gaussian, a rectangular, and an integrate-and-dump.

Gaussian filter This Gaussian filter is implemented similar to the pre-detection filter. Again, the parameter L_T is equal to 4. We represent the lowpass 3dB bandwidth of $h_{lp}(t)$ by B_{lp}. Two filters used in this study are those with B_{lp} of $0.45R$ denoted by GAUS45 and $0.7R$ denoted by GAUS70. Figure 3-3 displays a 31-tap GAUS70 filter.

Rectangular (REC) filter We design an FIR rectangular filter using the Parks-McClellan algorithm. The peak error is chosen to be less than 10^{-3} in both passband and stopband.

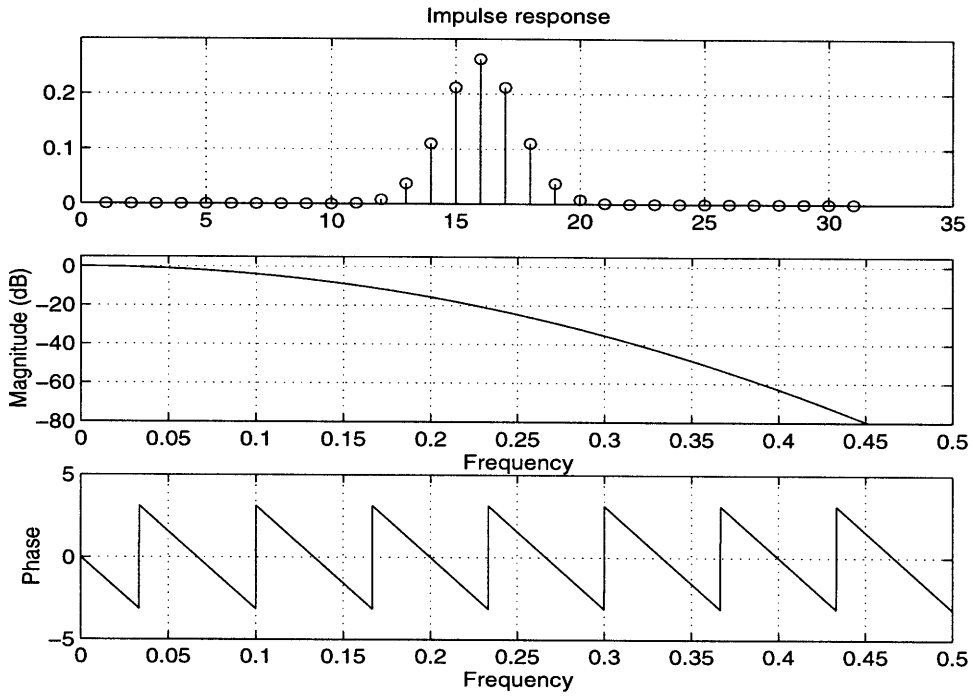

Figure 3-3: Impulse and frequency response of a 31-tap Gaussian filter with $B_{lp} = 0.7R$ (GAUS70).

The stopband attenuation is approximately 60 dB. We select the transition band to be between $0.2R$ and $0.8R$. The filter length is $6n_s + 1$ which results in a group delay of $3n_s$ samples. Figure 3-4 shows the impulse and frequency response of a 49-tap rectangular filter.

Integrate-and-dump (I&D) filter Integrate-and-dump filter is used extensively in the LD detection because of its simple design and good performance. The impulse response of the I&D filter is

$$h_{I\&D}(t) = \begin{cases} \frac{1}{T}, & 0 \leq t < T \\ 0, & \text{otherwise} \end{cases}$$

where the amplitude is scaled so that the magnitude response at DC is 1. The discrete-time I&D filter is obtained by sampling $h_{I\&D}(t)$. Figure 3-5 displays an impulse and frequency response of the I&D filter.

Magnitude responses of post-detection filters Magnitude responses of the four filters are shown in Figure 3-6. The frequency is normalized as suggested in section 3.1.1. From Figure 3-6, the REC filter has the sharpest transition while the GAUS70 has the flattest.

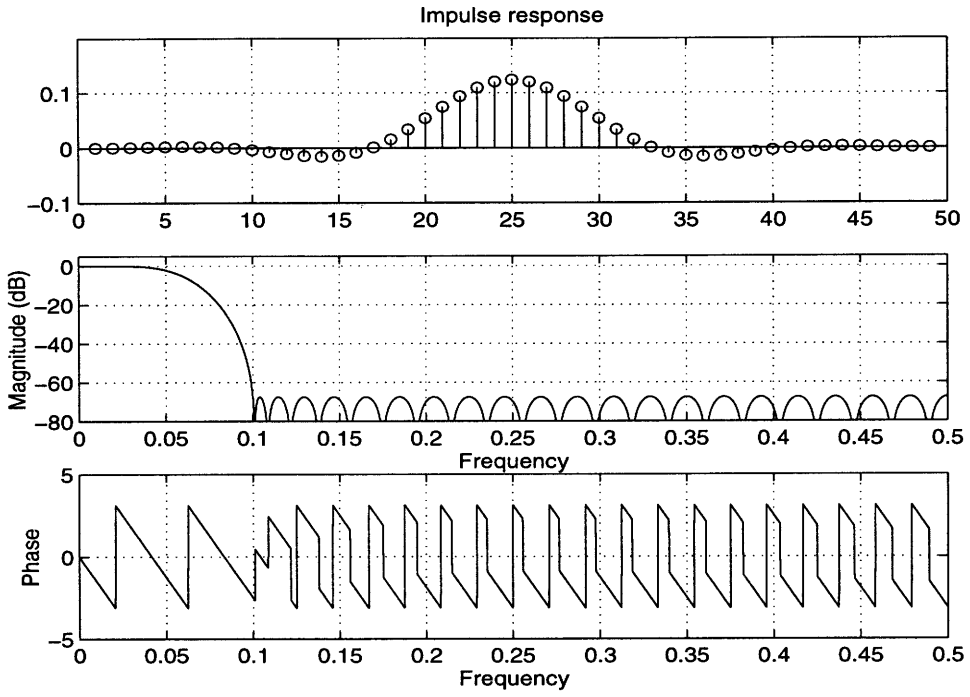

Figure 3-4: Impulse and frequency response of a 49-tap FIR rectangular filter (REC).

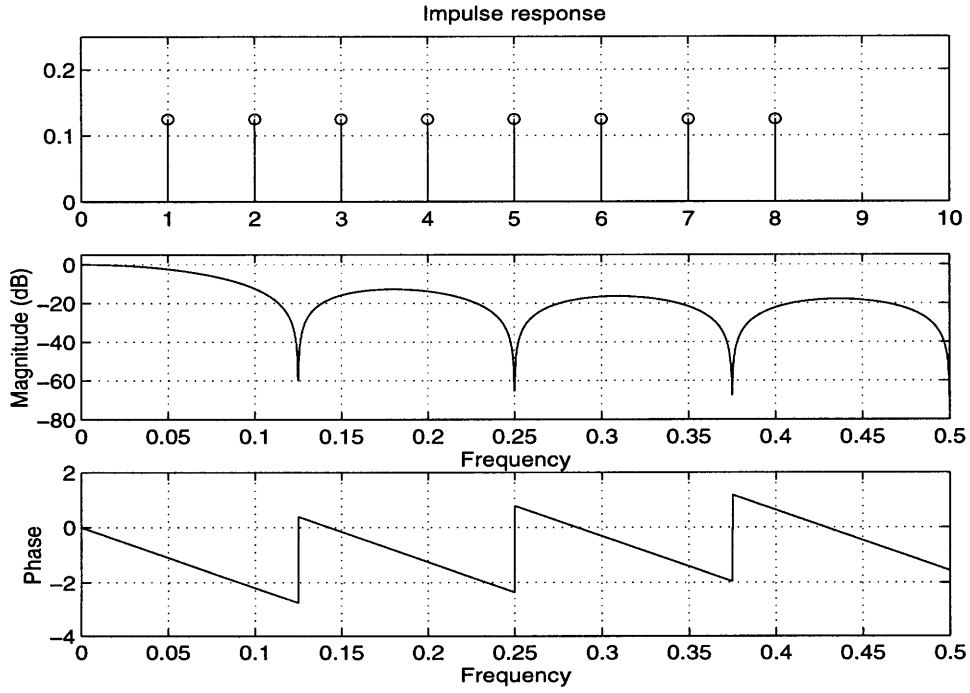

Figure 3-5: Impulse and frequency response of an integrate-and-dump filter (I&D).

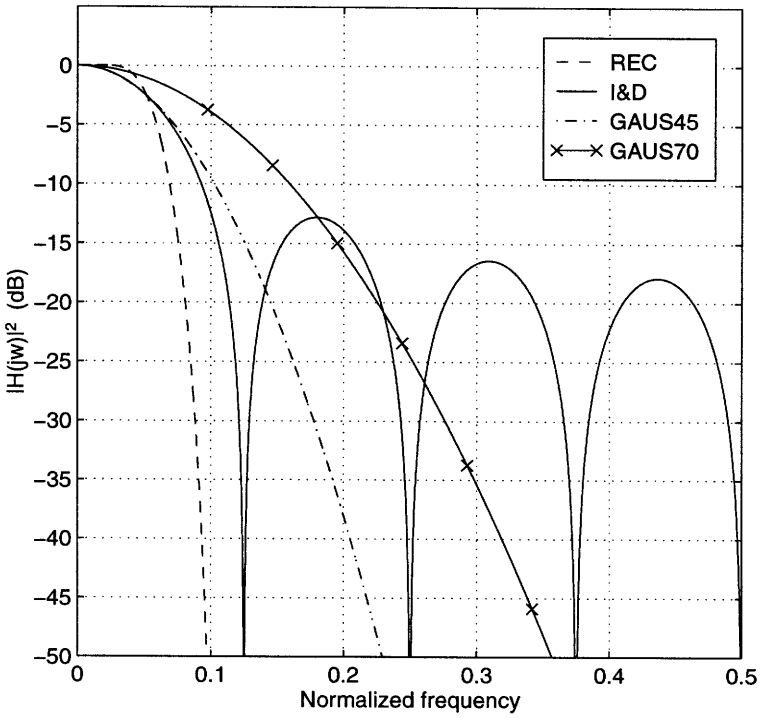

Figure 3-6: Magnitude responses of GAUS45, GAUS70, REC, and I&D filters.

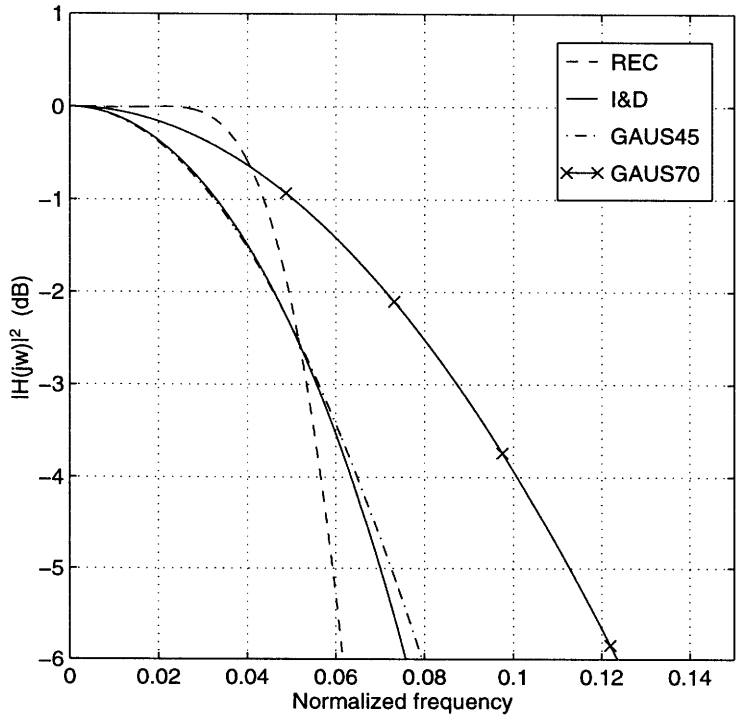

Figure 3-7: Magnitude responses of GAUS45, GAUS70, REC, and I&D filters in a finer scale.

The magnitude response of the GAUS45 filter lies between the two curves. The I&D filter has nulls at integer multiples of the symbol rate R.

Finally, Figure 3-6 is displayed in a finer scale in Figure 3-7. The responses of I&D and GAUS45 are the same until f is approximately 0.0625 ($0.5R$). As a result, the 3dB bandwidths of the two filters are almost identical. The REC filter has the smallest bandwidth while the GAUS70 has the largest.

3.2 Illustration of Non-coherent GMSK Demodulation

We now present examples of GMSK demodulation using the three non-coherent methods. For simplicity, we assume that the received signal is noise-free. Two post-detection filters considered are GAUS70 (Figure 3-3) and REC (Figure 3-4). A sequence of random input bits with equally likely probability is displayed in the top part of Figure 3-8. The phase waveforms before and after the Gaussian pre-detection filter are shown in the bottom of Figure 3-8. From the figure, $\theta[k]$ increases by roughly $\pi/2$ when the input bit is positive and decreases by the same amount when the input bit is negative. In addition, $\theta[k]$ differs from $\mu[k]$ only when the input bit reverses its sign. The difference between $\theta[k]$ and $\mu[k]$ at other time is very small.

For the LD receiver, the output of the discriminator, $\mu[k] - \mu[k-1]$, and the post-detection filtered outputs are displayed in the top and bottom part of Figure 3-9. Similar plots are shown in Figure 3-10 for the DD receiver. Outputs of three PLL receivers are displayed in Figure 3-11, 3-12, and 3-13.

The demodulated waveforms of all three PLL receivers display overshoots which do not occur in the outputs of the LD and DD receivers. Furthermore, the output of the PLL receiver with $\zeta = 0.4$ oscillates before it reaches a steady-state. We note that both overshoots and ringings are common characteristics of second-order linear systems. Because the PLL receiver is a non-linear system which can be approximated by a linear system, we therefore observe these characteristics in the demodulated outputs.

3.3 Performance in AWGN

We are interested in the comparative performance of the PLD detection versus the LD and DD detection in AWGN environment. To simplify the problem, the 31-tap FIR Gaussian

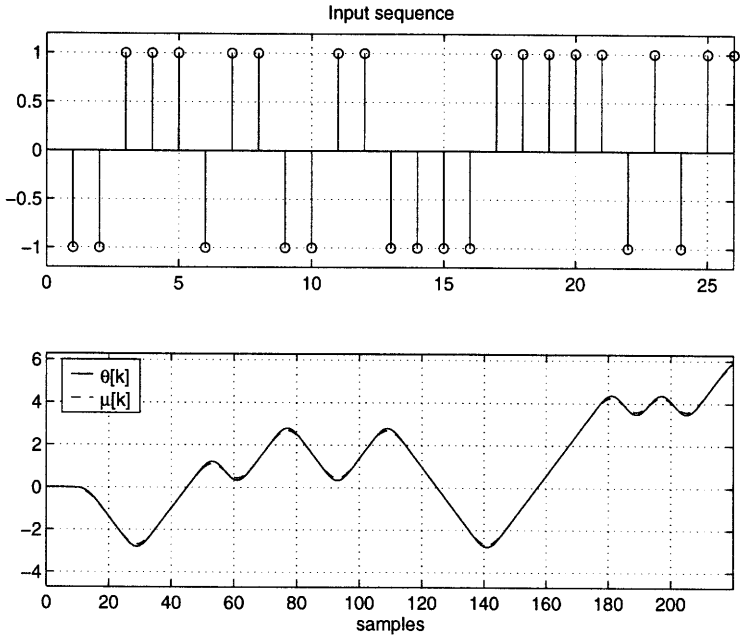

Figure 3-8: GMSK input bit sequence and phase waveforms.

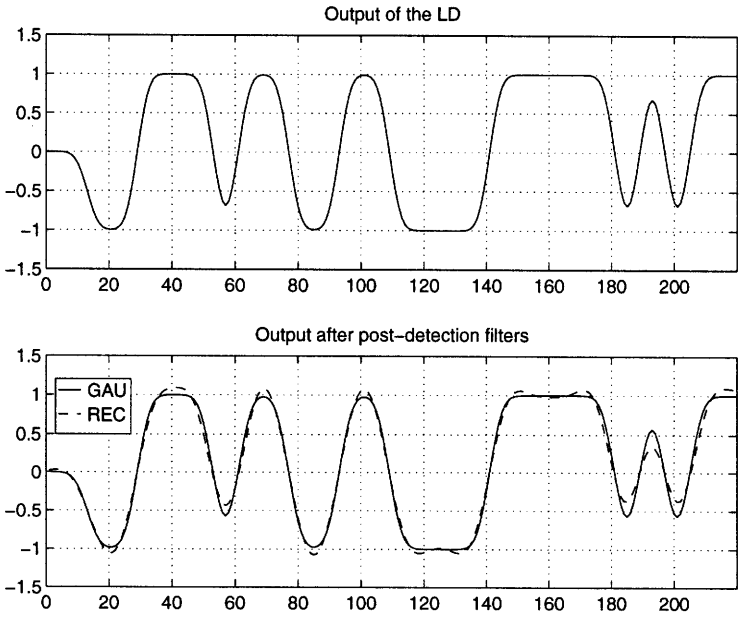

Figure 3-9: Output of an LD receiver.

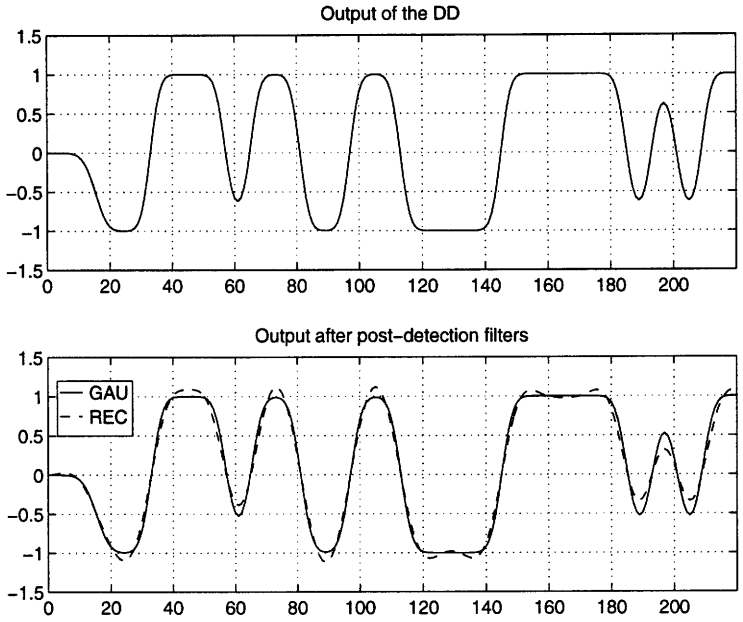

Figure 3-10: Output of a DD receiver.

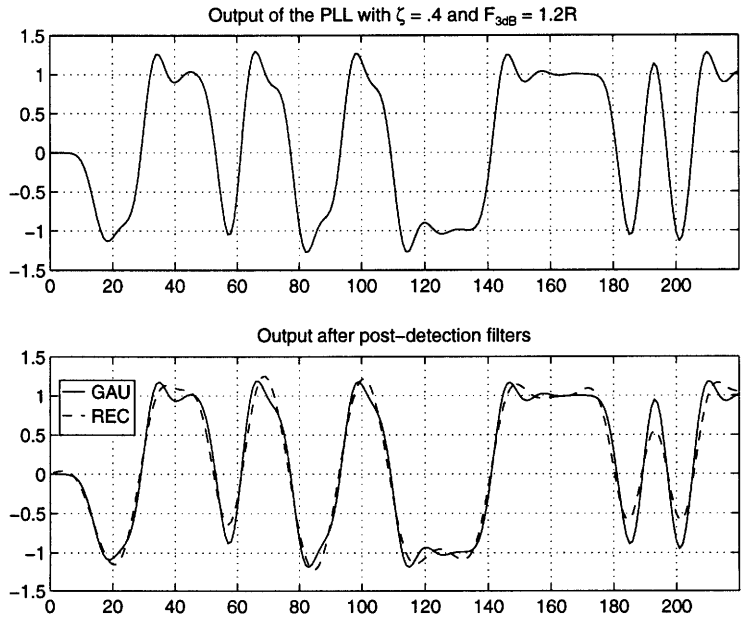

Figure 3-11: Output of a PLL receiver ($\zeta = 0.4$ and $F_{3dB} = 1.2R$).

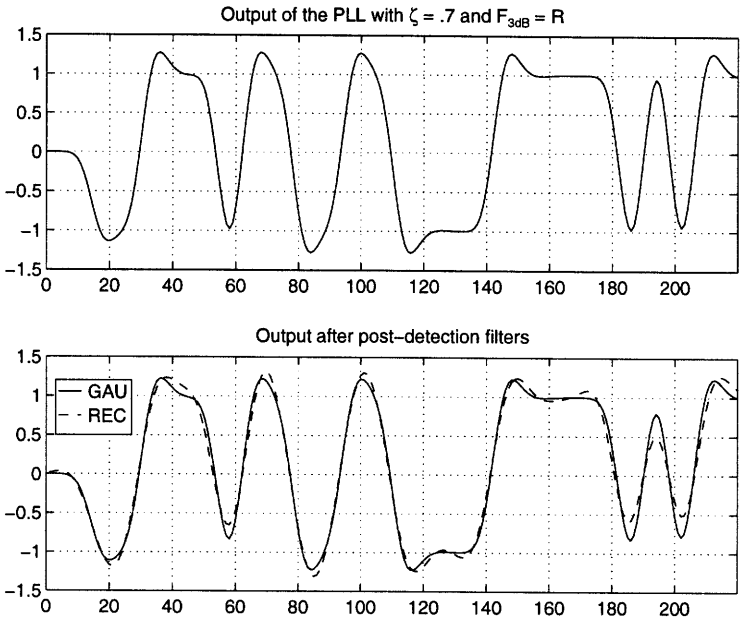

Figure 3-12: Output of a PLL receiver ($\zeta = 0.7$ and $F_{3dB} = R$).

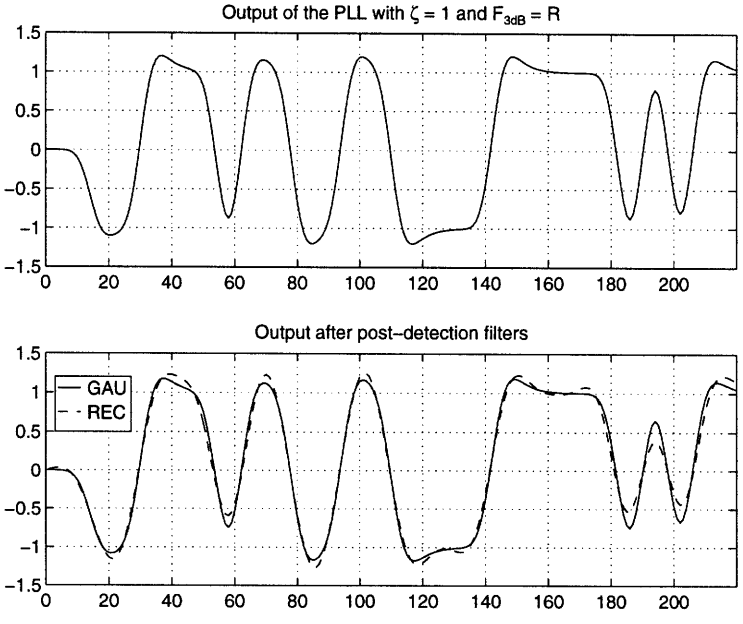

Figure 3-13: Output of a PLL receiver ($\zeta = 1$ and $F_{3dB} = R$).

filter with $B_{IF} = 1.1R$ (Figure 3-2) is chosen for pre-detection filtering. This particular choice of B_{IF} is known to be the optimal value for differential detection of GMSK with $B_tT = 0.5$ at $P_e = 10^{-3}$ [30]. Furthermore, a typical noise bandwidth of this filter is on the same order as that of a surface acoustic wave (SAW) filter used in DECT receivers. Our goal is to find a set of PLL receivers that perform better than the DD receiver, given the best condition for the latter. Also, we note that the optimal value of B_{IF} for the LD detection is not presented in literature.

It is true that this particular choice of pre-detection filter is unlikely to be the optimal pre-detection filter for PLL detection. In fact, the optimal pre-detection filter may depend on PLL parameters, post-detection filter, and error probability level. Given the number of parameters involved, the task of finding the optimal receiver by simulation is formidable. Therefore, we proceed by selecting B_{IF} to the value typical in practice.

We start by first simulating error probabilities of the LD and DD receivers and confirm our results with those from [26], [29], and [30]. PLL receivers with various values of ζ and F_{3dB} are then simulated. For post-detection, we consider GAUS70, GAUS45, and REC filters. Unless specified otherwise, we compare all error performances at $P_e = 10^{-3}$, which is the target BER for DECT receiver [19].

3.3.1 LD receiver

The performance of LD detection with several post-detection filters is shown in Figure 3-14. The theoretical result, displayed in the solid line, is obtained from (2.27) by evaluating (2.24) and (2.25) numerically. The simulated BER of the LD detector with I&D agrees well with the theoretical result. The LD detector with REC performs the same as the LD with I&D at low E_b/N_o, while the LD with GAUS45 performs slightly worse. At $P_e = 2 \cdot 10^{-3}$, the receiver with GAUS70 performs worse than the LD with I&D by 1.3 dB. This is due to a slow roll-off of the GAUS70 filter illustrated in Figure 3-6. Lastly, we note that the detection without post-detection filtering results in a 3 dB loss relative to the theoretical performance of the receiver with I&D. We do not include its plot in the figure.

3.3.2 DD receiver

Figure 3-15 shows the performance of DD receivers with various post-detection filters. The simulated BERs of the DD with GAUS45, GAUS70, REC, and no post-detection filter

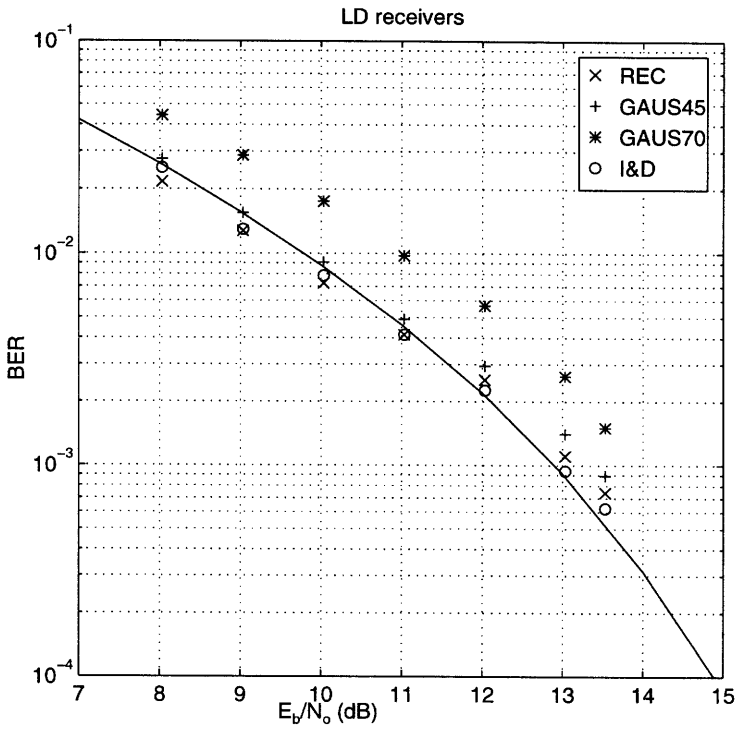

Figure 3-14: Performance of LD receivers in AWGN environment.

(NONE) are compared to that obtained from evaluating (2.32). The performance of the DD with NONE and GAUS70 is close to the theoretical result. The performance loss of the receiver with GAUS45 is 1 dB, while the loss of that with REC is 2 dB.

This result agrees with our observation in Section 2.2. The role of post-detection filter in differential detection is to get rid of the second harmonic term. In complex baseband representation, this term is zero. Therefore, inserting an extra filter at the output introduces more ISI. The receivers with narrow-bandwidth filters, thus, do not perform as well as those with broader filters or without any filter. Because of its sharpest attenuation, the REC filter gives the worst performance.

3.3.3 PLL receiver

For each post-detection filter, PLL receivers with ζ from 0.4 to 2 and F_{3dB} from $0.6R$ to $1.2R$ are simulated at $E_b/N_o = 11$ dB. We then select those receivers of interest and simulate their error probabilities for the whole range of E_b/N_o. The results are described in this section.

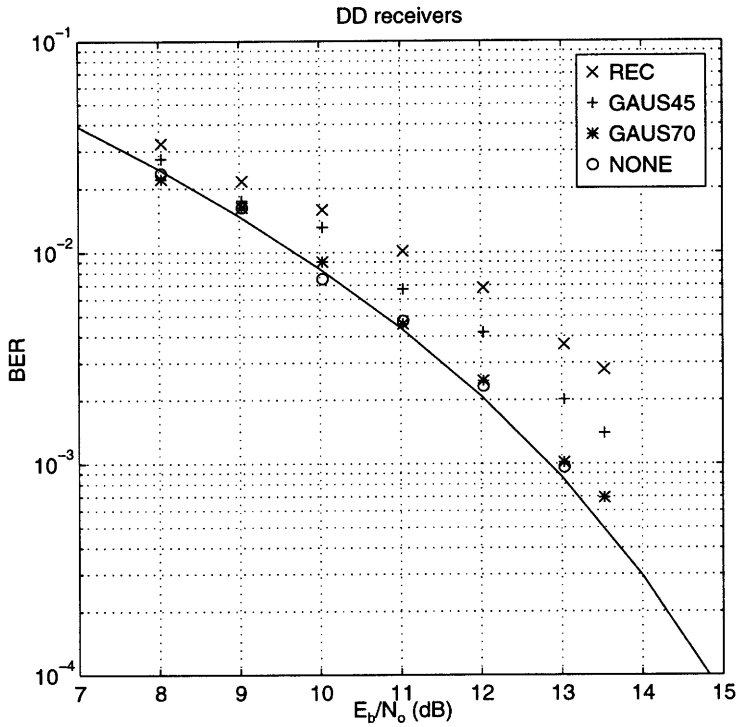

Figure 3-15: Performance of DD receivers in AWGN environment.

• **Receiver with GAUS70 filter** The performance of PLL receivers with GAUS70 is shown in Figure 3-16. Compared to the theoretical result of differential detection in Figure 3-15, these PLL receivers perform worse. The best performance (in $*$'s), obtained with $\zeta = 1$ and $F_{3dB} = 0.6R$, is still worse than that of the DD detection by roughly 0.5 dB. Again, the poor performance of these receivers is a result of the slow roll-off characteristic of GAUS70. Recall that the LD receiver with GAUS70 also performs worse than that with I&D by 1.3 dB. This finding suggests the use of post-detection filter with a narrower bandwidth.

• **Receiver with GAUS45 filter** The performance of PLL receivers with GAUS45 is simulated and plotted in Figure 3-17. Both receivers with $\zeta = 0.7$, $F_{3dB} = R$ and $\zeta = 1$, $F_{3dB} = R$ perform better than the DD receiver by 0.3 dB. It is interesting that as GAUS70 is replaced by GAUS45, the improvement in performance of each receiver is different. The PLL receiver with $\zeta = 0.7$ and $F_{3dB} = R$ gains 1.5 dB, while the PLL with $\zeta = 1$ and $F_{3dB} = R$ gains 0.9 dB.

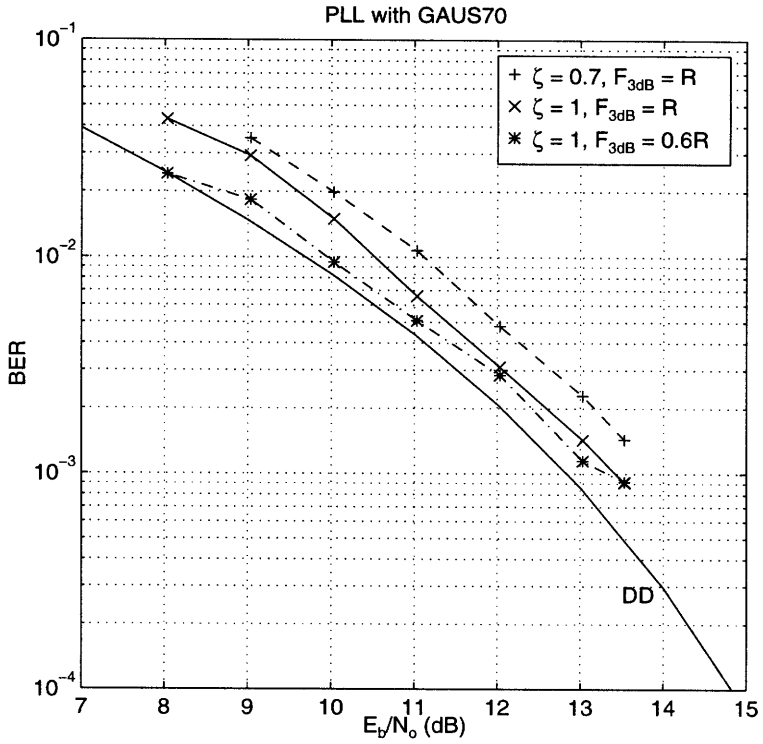

Figure 3-16: Performance of PLL receivers with GAUS70 in AWGN environment.

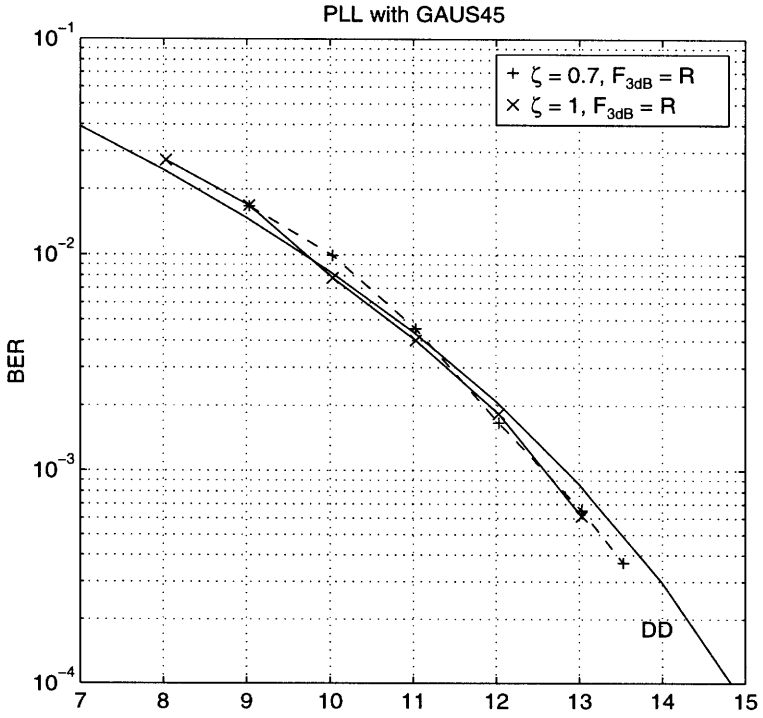

Figure 3-17: Performance of PLL receivers with GAUS45 in AWGN environment.

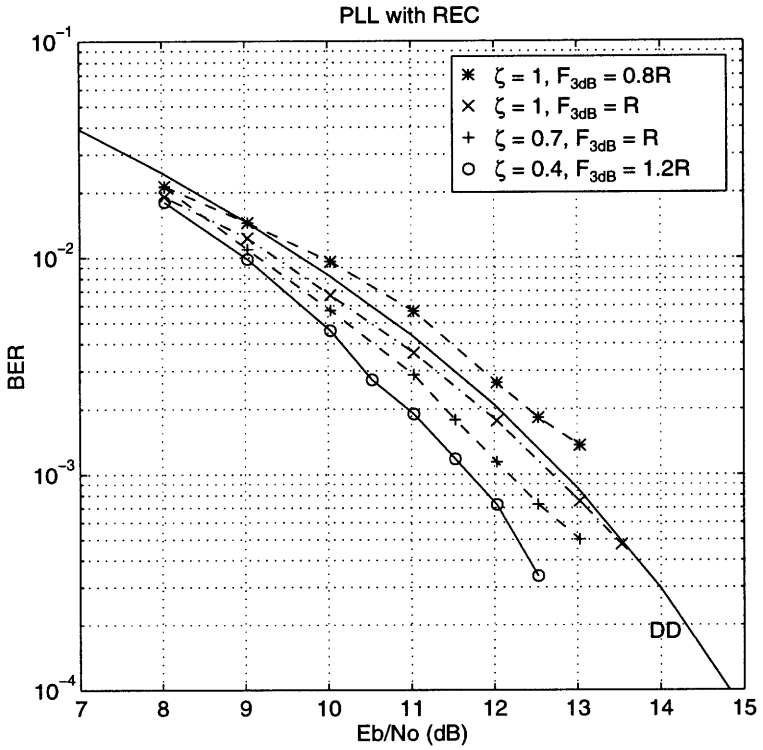

Figure 3-18: Performance of PLL receivers with REC in AWGN environment.

• **Receiver with REC filter** Figure 3-18 displays the performance of PLL receivers with the rectangular (REC) post-detection filter. At low E_b/N_o, the BERs are roughly the same for all four receivers. The difference becomes noticeable when $E_b/N_o \geq 10$ dB. The best result requiring E_b/N_o of 11.7 dB at $P_e = 10^{-3}$ is observed with $\zeta = 0.4$ and $F_{3dB} = 1.2R$. Its gain over the LD with I&D and the DD receivers is 1.2 dB. The receiver with $\zeta = 0.7$ and $F_{3dB} = R$ is better than both the LD and DD receivers by 0.7 dB. The receiver with $\zeta = 1$ and $F_{3dB} = R$ performs slightly better, while the last receiver with $\zeta = 1$ and $F_{3dB} = 0.8R$ performs worse by 0.5 dB.

From Figure 3-16 to 3-18, the error performance of the PLL receivers depends on post-detection filtering. The performance of the receivers with the same PLL parameters changes when a different post-detection filter is used. For example, the improvement of 1 dB at $P_e = 2 \cdot 10^{-3}$ is achieved when we replace the GAUS45 filter with the REC filter in the receiver with $\zeta = 0.7$ and $F_{3dB} = R$. In the next section, we study the effects of ζ and F_{3dB} on the error performance of PLL receivers with both Gaussian and rectangular post-detection filters.

Effects of ζ and F_{3dB} on PLL detection In this study, error probabilities of receivers with the same F_{3dB} are simulated for different ζ at $E_b/N_o = 11$ dB, and vice versa. Due to the poor performance of the PLL receivers with GAUS70, only those with GAUS45 and REC are considered.

• **Receiver with GAUS45** In Figure 3-19, the error probabilities of the PLL receivers are plotted as a function of ζ. Three loop bandwidths are chosen: $0.8R$ ($*$'s), R (+'s), and $1.2R$ (o's). From the figure, all receivers with $\zeta = 0.4$ perform poorly. For each F_{3dB}, the error probabilities of receivers also fluctuate when $\zeta < 1$. The difference in performance, however, reduces as we increase ζ. The performances at $\zeta = 2$ are almost identical for all three values of F_{3dB}.

Furthermore, we note that the optimal value of ζ differs for each F_{3dB}. While $\zeta = 1$ is best for the receivers with $F_{3dB} = R$, the best performance for the receiver with $F_{3dB} = 0.8R$ is obtained when $\zeta = 0.6$. For $F_{3dB} = 1.2R$, the receiver with $\zeta = 2$ provides the minimum error probability.

We now investigate the effects of F_{3dB} on the error performance. Shown in Figure 3-20 as a function of normalized $F_{3dB}T$, the performances of receivers with $\zeta = 2$ are the same for all values of F_{3dB}. In addition, all receivers with small ζ and $F_{3dB} > R$ perform poorly. The best performance for the PLL detection with GAUS45 is obtained with $\zeta = 1$ and $F_{3dB} = R$.

• **Receiver with REC** In Figure 3-21, the effects of ζ on PLL receivers with REC are displayed in the same fashion as Figure 3-19. Similar to the GAUS45 case, we observe a fluctuation of BERs for each F_{3dB} at low ζ. However, unlike the receiver with GAUS45, the receivers with low ζ perform well, especially when $F_{3dB} \geq R$. In fact, the best result is obtained with $\zeta = 0.4$ and $F_{3dB} = 1.2R$.

In Figure 3-22, the effects of F_{3dB} are somewhat opposite from the GAUS45 case. The receivers with $F_{3dB} = 1.2R$ perform better than those with F_{3dB} of $0.8R$. Those with $F_{3dB} = 0.8R$ perform poorly for all values of ζ. Also, it is interesting that the performances at $F_{3dB} = 1.2R$ are in order, from the receiver with the smallest ζ to the largest ζ. However, the opposite result holds for the receivers with GAUS45.

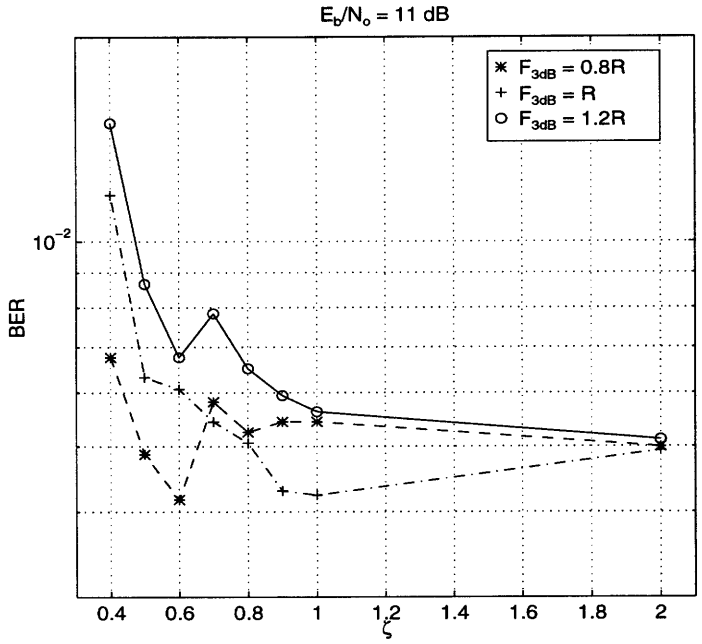

Figure 3-19: Performance of PLL receivers with GAUS45 at $E_b/N_o = 11$ dB, as a function of ζ.

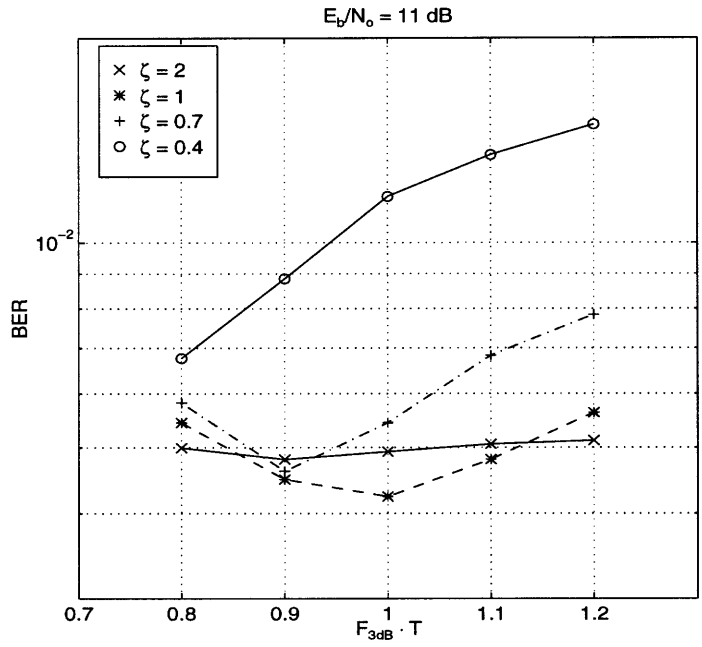

Figure 3-20: Performance of PLL receivers with GAUS45 at $E_b/N_o = 11$ dB, as a function of F_{3dB}.

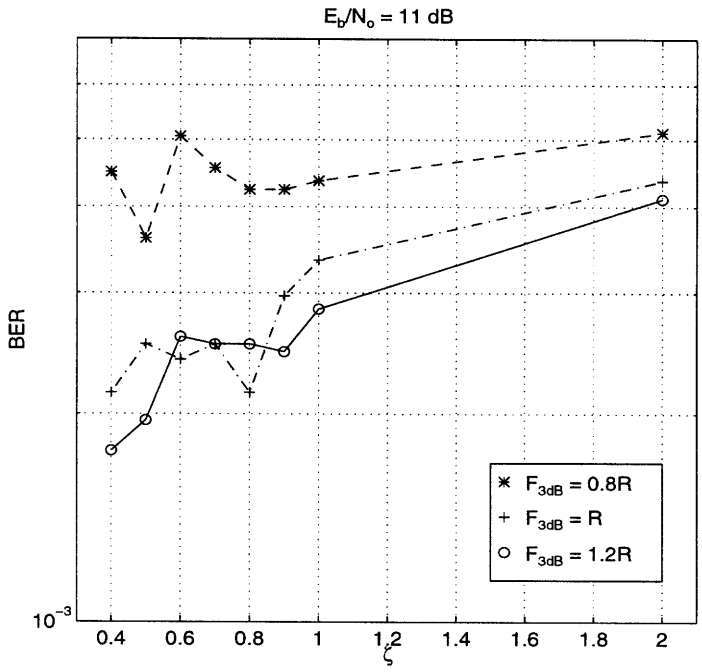

Figure 3-21: Performance of PLL receivers with REC at $E_b/N_o = 11$ dB, as a function of ζ.

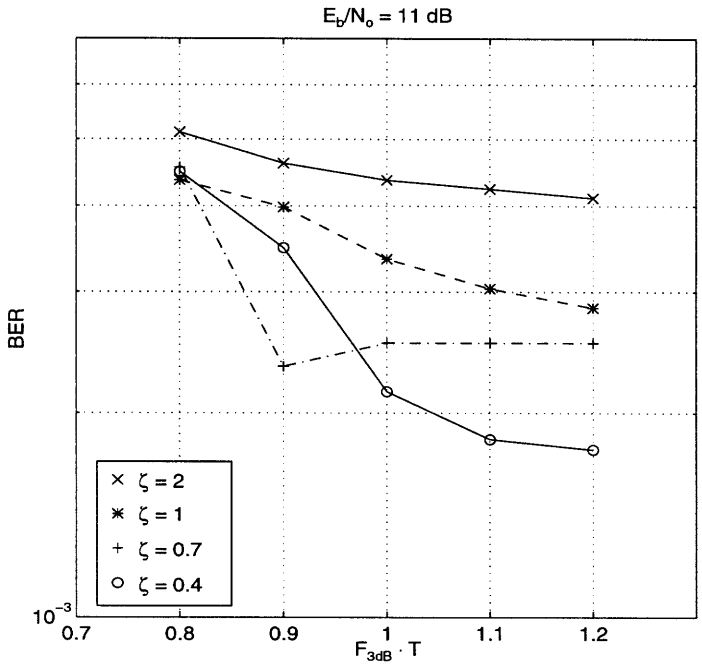

Figure 3-22: Performance of PLL receivers with REC at $E_b/N_o = 11$ dB, as a function of F_{3dB}.

Result analysis From the results, the simulated BERs of the PLL receivers depend strongly on ζ and F_{3dB}. In general, the effects of ζ and F_{3dB} on the performance vary, depending on post-detection filters. However, there are also some similarities. We explain these similarities using the linearized PLL model.

First, Figure 3-19 and 3-21 show that the BERs of the receivers with GAUS45 and REC fluctuate as a function of ζ, when $\zeta < 1$. This is because of the underdamping characteristics of the PLL. From Figure 2-12, the transfer function $H_{PLD}(s)$ of an underdamped PLL has a very high peak, and its magnitude response varies significantly as a function of ζ. Since the characteristics of the demodulated output depend on the shape of this transfer function, the error probability of the receiver with $\zeta < 1$, therefore, fluctuates as we change ζ.

Second, for the receivers with $\zeta > 1$, there is only a small difference in the BERs for distinct values of F_{3dB}. For example, the BER curves of the receiver with $\zeta = 2$ in Figure 3-20 and 3-22 are relatively flat and independent of F_{3dB}. This is because, when $\zeta > 1$ and F_{3dB} is between $0.6R$ and $1.2R$, $H_{PLD}(s)$ are almost the same for f below R. After combining with a narrow-band post-detection filter such as GAUS45 or REC, the performance of the PLL receivers with $\zeta > 1$ is, therefore, less dependent on F_{3dB}.

Summary We simulate error probabilities of PLL receivers in AWGN environment with different ζ and F_{3dB} for three post-detection filters: GAUS45, GAUS70, and REC. The PLL receivers with GAUS70 perform poorly, while the receivers with GAUS45 perform slightly better than the LD and DD receivers. Using the rectangular filter (Figure 3-4), the PLL receivers provide the best performance. The best result obtained with $\zeta = 0.4$ and $F_{3dB} = 1.2R$ is better than that of the LD and DD receivers by 1.2 dB.

We then study the effects of ζ and F_{3dB} on the error performance of PLD detection with GAUS45 and REC. From Figure 3-19 - 3-22, we conclude that the simulated BERs depend strongly on ζ and F_{3dB}, and the effects of ζ and F_{3dB} on the PLD detection with different post-detection filtering vary. Choosing the right combination of ζ and F_{3dB} for each particular post-detection filter is, therefore, crucial to achieve a good error performance.

3.4 Performance in Interference-limited Environments

3.4.1 Cochannel and adjacent channel interference

Up to this point, we have assumed that AWGN is the only source of channel's degradation. In reality, however, communication systems also operate in the presence of other interference sources. The interferer can be another type of signal sharing the same spectrum, or the same type coming from other users. In cellular systems, interference is a consequence of the frequency reuse concept where the same channel is reused in non-neighboring cells. Another example is Cellular Digital Packet Data (CDPD) system which shares spectrum with Advanced Mobile Phone System (AMPS).

There are two types of interferences. Cochannel interference (CCI) represents an interference which resides in the same channel as the desired signal, while adjacent channel interference (ACI) corresponds to an interference occupying nearby channels. General expression of the received signal in the presence of interference and AWGN is

$$r(t) = A\cos(2\pi f_c t + \theta(t) + \theta_o) + \sum_{i=1}^{m} s_{C_i}(t) + \sum_{j=1}^{l} s_{A_j}(t) + n(t) \tag{3.4}$$

where $s_{C_i}(t)$ and $s_{A_j}(t)$ are CCI and ACI interfering signals. When all interferers are CPM signals, we obtain

$$r(t) = A\cos(2\pi f_c t + \theta(t) + \theta_o) + \sum_{i=1}^{m} \gamma_i \cos(2\pi(f_c + \Delta f_i)(t - \tau_i) + \phi_i(t - \tau_i) + \theta_i) + n(t) \tag{3.5}$$

in which we denote the amplitude and the phase shift of each interference by γ_i and θ_i respectively. The ratio of the signal power and the interference power is called the carrier-to-interference ratio (CIR). The phase of the interference, $\phi_i(t)$, is defined similarly to $\theta(t)$ in (1.5). The terms τ_i and Δf_i represent a time delay and a difference in the carrier frequency between the i^{th} interferer and the desired signal. In CCI, Δf_i is equal to 0.

Performance of non-coherent CPM receivers in the presence of ACI and CCI is discussed in [34, 35, 36]. LD detection of GMSK with no fading has been analyzed in the context of spectral efficiency in [34]. Wickert and Jacobsmeyer have investigated the performance of GMSK receiver based on LD in flat fading Rayleigh channel [35]. In [36], Korn has studied error probability of partial-response CPM with the LD and DD detection in frequency-

selective Rayleigh fading channel and has found that, at high CNR (above 20 dB), the LD detector performs better than both the one-bit and two-bit DD detectors in the presence of CCI. However, we note that all three studies are done without post-detection filtering. Therefore, their results can not be directly compared to ours.

3.4.2 Simulation results

We investigate, in this study, the performance of PLL receivers in the presence of only one interferer. The simulations are done within the DECT framework. Both the desired and the interfering signal employ GMSK modulation with $B_tT = 0.5$. The two input sequences are independent from each other, and each bit is equiprobable. The interference phase shift θ_i is uniformly distributed in $[-\pi, \pi]$, while the delay τ_i is between $[0, T]$. In addition, Δf in ACI simulations is set to $1.5R$ – a frequency spacing of DECT.

All simulations are done on static channels with no multipath fading. An AWGN with CNR = 20 dB is included; this is the ratio measured after the pre-detection filter. In the DECT standard, the required CIR to achieve $P_e = 10^{-3}$ in a single channel, corrupted by AWGN with CNR = 20 dB, must be less than 9 dB [19]. That is, the ratio between the signal and the cochannel interference power to achieve $P_e = 10^{-3}$ is less than 9 dB.

Three PLL receivers considered in this study are

$$\begin{aligned}
&\text{PLL1} \quad \zeta = 0.4, F_{3dB} = 1.2R \\
&\text{PLL2} \quad \zeta = 0.7, F_{3dB} = R \\
&\text{PLL3} \quad \zeta = 1, \quad F_{3dB} = R.
\end{aligned}$$

These are the receivers which perform well in AWGN. Pre-detection filter is the Gaussian filter with $B_{IF} = 1.1R$. Post-detection filters are GAUS45, GAUS70, and REC. The LD receiver with I&D and the DD receiver with NONE are also simulated.

CCI The comparative performance of LD, DD, and PLL receivers as a function of CIR is shown in Figure 3-23. The best performance is by the PLL3 with GAUS45 requiring CIR = 7.5 dB at $P_e = 10^{-3}$. The PLL1 with REC comes next, followed by the LD and DD receivers. The LD with I&D requires 8 dB, while the DD with NONE and the PLL2 with GAUS45 require roughly 8.2 dB.

Figure 3-24 to 3-26 illustrate the performance of each demodulator with different post-

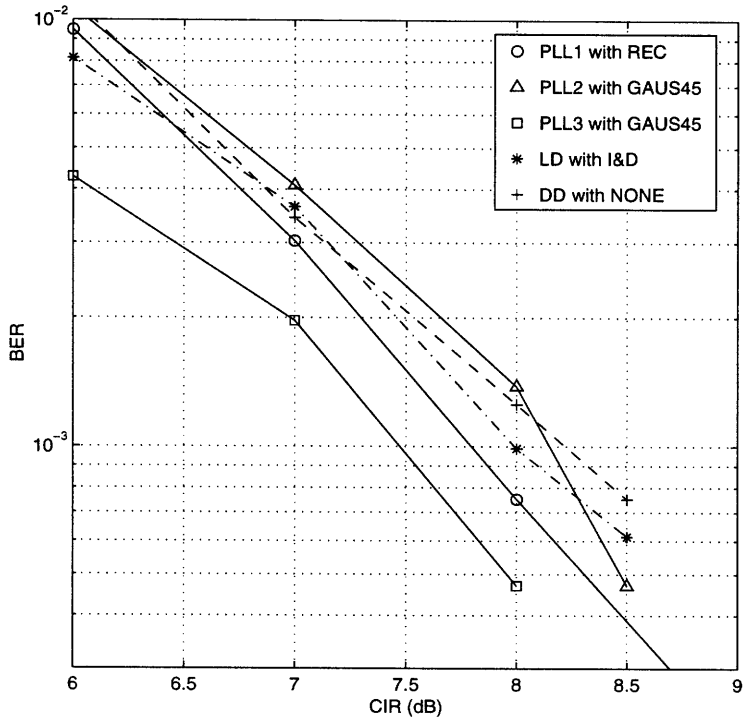

Figure 3-23: Performance in CCI environment.

detection filters. The performance of the LD detection with I&D and GAUS45 is roughly the same, with the latter being worse at high CIRs. The LD receiver with REC, however, performs poorly. Note that the three receivers perform roughly the same in AWGN. In the DECT context, both the LD with I&D and GAUS45 satisfy the requirement previously mentioned.

For DD, only the DD with NONE satisfies the criteria. Despite similar performance in AWGN, the DD with GAUS70 performs worse than the DD with NONE by 1 dB in this test. Furthermore, all the DD receivers with narrow-bandwidth filters perform poorly similar to the AWGN case.

For the PLL2 and PLL3, the GAUS45 post-detection filter provides the best results, while the PLL1 requires the REC filter. All receivers with GAUS70 perform poorly; therefore, their results are not included. Note that the gap in performance between the receivers with GAUS45 and REC depends on the PLL parameters. The gap is 1 dB for PLL2 and 2 dB for PLL3.

In summary, both the PLL3 ($\zeta = 1, F_{3dB} = R$) with GAUS45 and PLL1 ($\zeta = 0.4, F_{3dB} = 1.2R$) with REC provide improved performance over all LD and DD receivers. Six receivers

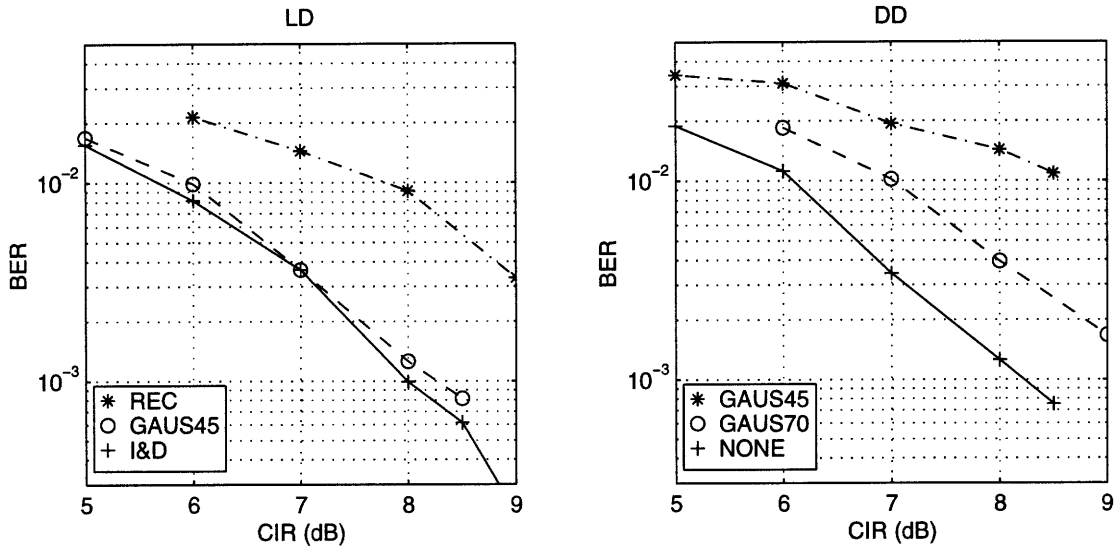

Figure 3-24: Performance of LD and DD receivers in CCI environment.

which satisfy the DECT requirement are PLL1 with REC, PLL2 with GAUS45, PLL3 with GAUS45, LD with I&D, LD with GAUS45, and DD with NONE. In the ACI study, we emphasize on these receivers.

ACI The comparative performance of the six receivers is shown in Figure 3-27 as a function of CIR. The best performance is by the PLL3 with GAUS45, requiring CNR = 5 dB at $P_e = 10^{-3}$. The PLL2 with GAUS45 achieves the same performance at high CNR. The PLL1 with REC performs better than the LD with GAUS45 when CIR > 5 dB. Both the DD with NONE and the LD with I&D perform worse than the PLL3 with GAUS45 by 6 dB.

The drastic difference in performance between the LD with I&D and the LD with GAUS45 can be explained by spectral characteristics of the receivers. When the desired signal is corrupted by ACI, its spectral density increases at frequencies near Δf. This increase also occurs in the spectrum of the phase, although the exact expression is not known. In the LD detection, the high frequency spectrum of the phase is boosted by the discriminator. To achieve a good performance, the post-detection filter must attenuate the unwanted spectrum as much as possible. By looking at the magnitude response of the I&D

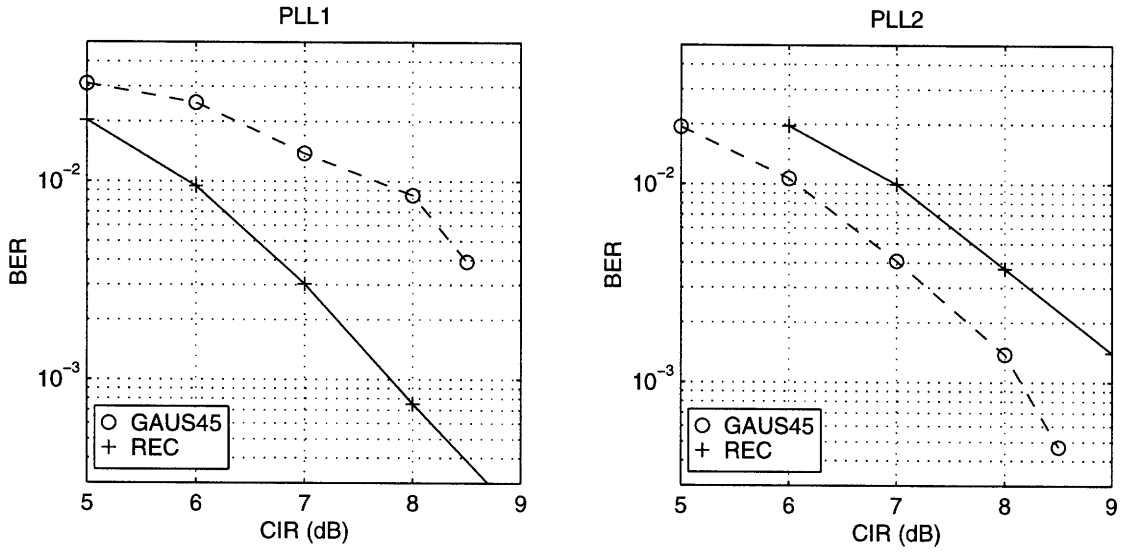

Figure 3-25: Performance of PLL1 and PLL2 receivers in CCI environment.

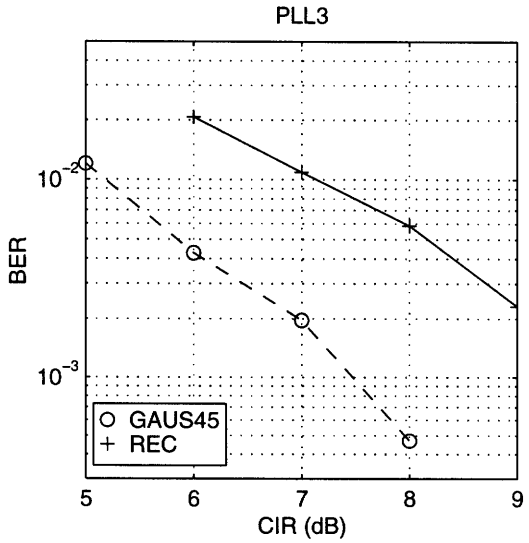

Figure 3-26: Performance of PLL3 receivers in CCI environment.

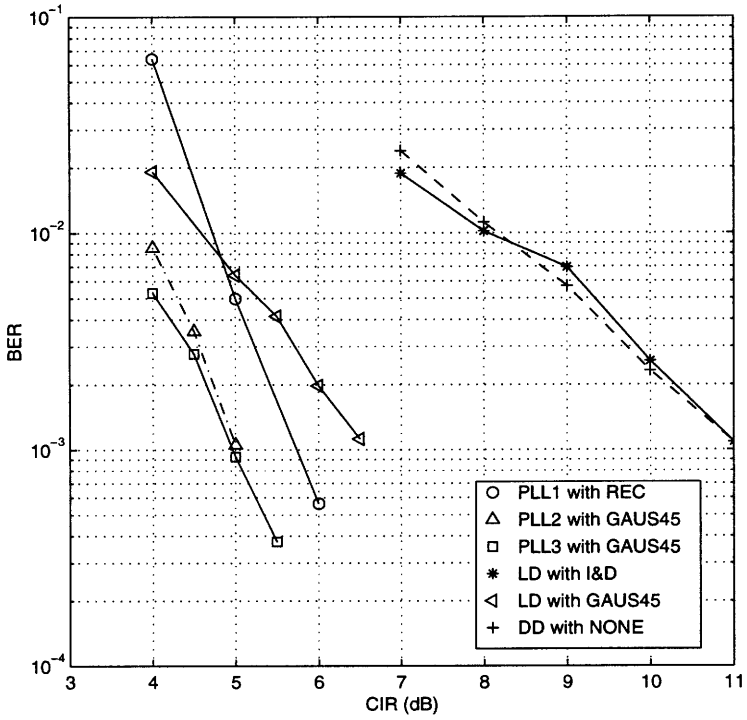

Figure 3-27: Performance in ACI environment.

filter in Figure 3-6, we can see that the attenuation of spectrum near $1.5R$ is less than 15 dB. At the same frequency range, the GAUS45 provides 35 dB attenuation. This results in a 4.5 dB difference in performance between the two LD receivers.

In the PLD detection, the loop transfer function provides additional lowpass filtering to the unwanted spectrum. This results in a better performance compared to the LD and DD detection. Using the same post-detection filter, the PLL2 and PLL3 with GAUS45 outperform the LD with GAUS45 by 1.5 dB.

In the presence of ACI, all three PLL receivers outperform the LD with I&D and DD with NONE receivers by 5-6 dB. This major improvement is due to two factors: the additional filtering by PLL and the poor frequency response of the I&D filter.

3.5 Summary

Table 3.1 summarizes the comparative performance of PLL, LD, and DD receivers in AWGN, CCI, and ACI environments. Each number indicates the receiver's improvement in the required CNR or CIR, to achieve $P_e = 10^{-3}$, over the LD detection with I&D. For

Table 3.1: Comparative performance of LD, DD, and PLL receivers in AWGN, CCI, and ACI tests.

Receiver	AWGN	CCI	ACI
PLL1 ($\zeta = 0.4, F_{3dB} = 1.2R$) with REC	1.19	0.2	5.29
PLL2 ($\zeta = 0.7, F_{3dB} = R$) with GAUS45	0.32	-0.15	6.0
PLL3 ($\zeta = 1, F_{3dB} = R$) with GAUS45	0.31	0.52	6.1
DD with NONE	-0.08	-0.23	0
LD with I&D	–	–	–
LD with GAUS45	-0.5	-0.26	4.52

comparison, we use the theoretical BER of the LD with I&D in the AWGN test and the simulated BERs in the CCI and ACI tests.

From the table, the PLL receivers outperform LD and DD receivers in all cases except one (the PLL2 with GAUS45 in CCI test). The main improvement is in the ACI test where the PLL receivers outperform both the DD and LD with I&D receivers by 5-6 dB. The PLL3 with GAUS45 provides the best performance in both CCI and ACI tests, while the PLL1 with REC performs best in AWGN.

Therefore, both the PLL1 with REC and the PLL3 with GAUS45 are more attractive candidates for DECT receiver than the traditional LD and DD.

Advantages of PLL receivers We conclude this chapter by summarizing two advantages of using the PLL receiver for GMSK demodulation over the LD and DD receivers.

The first advantage is the improved performance of the PLL receiver – especially in the presence of ACI. In mobile radio applications, this leads to a larger cell coverage and power savings. Furthermore, its great performance in the ACI environment provides a possible relaxation of filtering requirements in a receiver front-end.

Secondly, the PLL receiver provides more flexibility to accommodate different operating conditions. By adjusting the loop parameters, one can obtain a good performance for any particular scenario. In practice, reconfiguration of these loop parameters is done easily by changing passive circuit elements of the loop filter. The PLD detection technique, therefore, provides two additional parameters for optimization, while the LD and DD detection do not have this option.

Chapter 4

CONCLUSIONS

We have investigated the performance of PLL receiver for GMSK modulation in AWGN and interference-limited environments. From the simulation results, we have observed that the receiver's error performance depends strongly on both the PLL parameters and the post-detection filter. In AWGN environment, the PLL receivers, using the rectangular filter (Figure 3-4), perform well; the largest gain over the theoretical performance of LD and DD detection is 1.2 dB. On the other hand, the performance using the Gaussian post-detection filter ($B_{lp} = 0.45R$) is best in the interference-limited environment. The performance improvement in ACI environment compared to the DD receiver and the LD receiver with an integrate-and-dump filter is up to 6 dB.

In mobile radio communications, this improvement could lead to a larger cell design and the power saving of the mobile unit. The implementation costs could, therefore, be reduced. Furthermore, easy reconfiguration of the PLL receiver provides flexibility in different operating conditions. These advantages make the PLL receiver a good candidate for GMSK demodulation in mobile radio applications.

Future works Possible extensions of the work presented in this thesis span different areas. First, the effect of the pre-detection filter should be investigated to address practical issues of receiver implementation. We are interested in performance comparison between receivers using different pre-detection filters, for example, the Gaussian filters with various B_{IF} and the SAW filter. Moreover, we suggest that the test should be done on several post-detection filters, including the Gaussian and rectangular filters.

Second, transient behaviors of the receiver should be studied. In this thesis, we have

assumed that the loop is always in lock, and therefore equation (2.34) can be reduced to (2.35). In practice, however, the PLL can only be locked in limited conditions, due to its non-ideal components. For example, the VCO has a maximum input limit, and the phase detector is only linear in a certain region [6]. The PLL receiver, therefore, requires some time to track the transmitted carrier frequency. Backgrounds on transient responses, linear, and non-linear tracking are given in [4] and [6].

Third, the performance in multipath fading channel should be studied. For mobile radio communications, Rayleigh fading channel is generally assumed. Although the analysis of the error performance is complicated, its simulation could be done by extending from our setup to include time-dispersion and amplitude fading.

Lastly, the results should be verified by empirical studies. In the DECT framework, Analog Devices has produced a transceiver, AD6411, based on the PLD detection. The damping and the loop bandwidth parameters can be adjusted easily because the loop filter is implemented externally by simple lumped circuits. It is interesting to see the comparison between the simulation and the experimental results. Furthermore, the experimental results of the PLL receivers could be compared with those of the LD or DD receivers. For example, Tjhung et al. conducted an experiment on the LD detection of CPFSK signals in Rayleigh fading channel [37].

Bibliography

[1] J. H. Roberts. *Angle Modulation.* Peregrinus, 1977.

[2] J. B. Anderson, T. Aulin, and C.-E. Sundberg. *Digital Phase Modulation.* Plenum Press, 1986.

[3] R. W. Lucky, J. Salz, and E. J. Weldon, Jr. *Principles of Data Communication.* McGraw-Hill, 1968.

[4] A. J. Viterbi. *Principles of Coherent Communication.* McGraw-Hill, 1966.

[5] J. Klapper and J. T. Frankle. *Phased-Locked and Frequency-Feedback Systems.* Academic Press, 1972.

[6] F. M. Gardner. *Phaselock Techniques.* Wiley, 1979.

[7] W. C. Lindsey and M. K. Simon. *Telecommunication Systems Engineering.* Dover, 1973.

[8] M. C. Jeruchim, P. Balaban, and K. S. Shanmugan. *Simulation of Communication Systems.* Plenum, 1992.

[9] F. M. Gardner and J. D. Baker. *Simulation Techniques: Model of Communication Signals and Processes.* Wiley, 1997.

[10] F. G. Stremler. *Communication Systems.* Addison-Wesley, 1990.

[11] T. S. Rappaport. *Wireless Communications.* Prentice Hall, 1996.

[12] Y. Akaiwa. *Introduction to Digital Mobile Communication.* Wiley, 1997.

[13] D. J. Goodman. *Wireless Personal Communications Systems.* Addison-Wesley, 1997.

[14] E. G. Sidiras. *Digital Demodulation of Continuous Phase Modulation.* Master thesis, Northeastern University, May 1995.

[15] J. G. Proakis and M. Salehi. *Communication Systems Engineering.* Prentice Hall, 1994.

[16] J. G. Proakis. *Digital Communications.* McGraw-Hill, 1995.

[17] A. V. Oppenheim and R. W. Schafer. *Discrete-time Signal Processing.* Prentice Hall, 1989.

[18] A. V. Oppenheim, A. S. Willsky, and I. T. Young. *Signals and Systems.* Prentice Hall, 1983.

[19] European Telecommunications Standards Institute. *Digital European Cordless Telephone Common Air Interface.* ETSI, 1996.

[20] S. O. Rice. Noise in FM receivers. In M. Rosenblatt, editor, *Time Series Analysis*, pages 394-422. McGraw-Hill, 1963.

[21] J. E. Mazo and J. Salz. Theory of error rates for digital FM. *Bell Syst. Tech. J.*, 45:1511-1535, Nov. 1966.

[22] S. Pasupathy. Minimum shift keying: A spectrally efficient modulation. *IEEE Commun. Mag.*, pages 14-22, July 1981.

[23] K. Murota and K. Hirade. GMSK modulation for digital mobile radio telephony. *IEEE Trans. Commun.*, COM-29:1044-1050, July 1981.

[24] C.-E. Sundberg. Continuous phase modulation. *IEEE Commun. Mag.*, 24:25-38, April 1986.

[25] N. A. B. Svensson and C.-E. Sundberg. Performance evaluation of differential and discriminator detection of continuous phase modulation. *IEEE Trans. Vehicular Tech.*, VT-35:106-117, August 1986.

[26] R. F. Pawula. On the theory of error rates for narrow-band digital FM. *IEEE Trans. Commun.*, COM-29:1634-1643, Nov. 1981.

[27] R. F. Pawula. Refinements to the theory of error rates for narrow-band digital FM. *IEEE Trans. Commun.*, COM-36:509-513, April 1988.

[28] R. F. Pawula, S. O. Rice, and J. H. Roberts. Distribution of the phase angle between two vectors perturbed by Gaussian noise. *IEEE Trans. Commun.*, COM-30:1828-1841, Aug. 1982.

[29] M. K. Simon and C. C. Wang. Differential versus limiter-discriminator detection of narrow-band FM. *IEEE Trans. Commun.*, COM-31:1227-1234, Nov. 1983.

[30] M. K. Simon and C. C. Wang. Differential detection of Gaussian MSK in a mobile radio environment. *IEEE Trans. Vehicular Tech.*, VT-33:307-320, Nov. 1984.

[31] G. K. Kaleh. A differentially coherent receiver for minimum shift keying signal. *IEEE J. Selected Areas Commun.*, SAC-7:99-106, Jan. 1989.

[32] G. K. Kaleh. Differentially coherent detection of binary partial response continuous phase modulation with index 0.5. *IEEE Trans. Commun.*, COM-39:1335-1340, Sep. 1991.

[33] S. Safavi, L. B. Lopes, P. E. Mogensen, and F. Frederiksen. A hierarchy of receiver options for DECT systems. *Proceeding of the 6th IEEE International Symposium on Personal, Indoor and Mobile Radio Communications (PIMRC 95)* , Toronto, Canada, Sept. 1995, pp. 1351-1356.

[34] O. Andrisano and N. Ladisa. On the spectral efficiency of CPM systems over real channel in the presence of adjacent channel and cochannel interference: A comparison between partial and full response systems. *IEEE Trans. Vehicular Tech.*, VT-39:89-100, May 1990.

[35] M. A. Wickert and J. M. Jacobsmeyer. GMSK receiver performance with narrowband FM interference on a cellular radio channel. *Proceeding of the 46th IEEE Vehicular Technology conference (VTC 96)* , Atlanta, GA., Apr. 1996, pp. 756-760.

[36] I. Korn. GMSK with frequency-selective Rayleigh fading and cochannel interference. *IEEE J. Selected Areas Commun.*, SAC-10:506-515, April, 1992.

[37] T. T. Tjhung, K. M. Lye, K. A. Koh, and K. B. Chang. Error rates for narrow-band digital FM with discriminator detection in mobile radio systems. *IEEE Trans. Commun.*, COM-38:999-1005, July, 1990.